J. Fluid Mech. (2000), *vol.* 412, *pp.* 125–160. Printed in the United Kingdom

Nonlinear effects in two-layer large-amplitude geostrophic dynamics. Part 1. The strong-beta case

By RICHARD H. KARSTEN AND GORDON E. SWATERS

Applied Mathematics Institute, Department of Mathematical Sciences,
and Institute for Geophysical Research, University of Alberta, Edmonton, T6G 2G1, Canada

(Received 6 January 1999 and in revised form 14 January 2000)

Baroclinic large-amplitude geostrophic (LAG) models, which assume a leading-order geostrophic balance but allow for large-amplitude isopycnal deflections, provide a suitable framework to model the large-amplitude motions exhibited in frontal regions. The qualitative dynamical characterization of LAG models depends critically on the underlying length scale. If the length scale is sufficiently large, the effect of differential rotation, i.e. the β-effect, enters the dynamics at leading order. For smaller length scales, the β-effect, while non-negligible, does not enter the dynamics at leading order. These two dynamical limits are referred to as *strong-β* and *weak-β* models, respectively.

A comprehensive description of the nonlinear dynamics associated with the strong-β models is given. In addition to establishing two new nonlinear stability theorems, we extend previous linear stability analyses to account for the finite-amplitude development of perturbed fronts. We determine whether the linear solutions are subject to nonlinear secondary instabilities and, in particular, a new long-wave–short-wave (LWSW) resonance, which is a possible source of rapid unstable growth at long length scales, is identified. The theoretical analyses are tested against numerical simulations. The simulations confirm the importance of the LWSW resonance in the development of the flow. Simulations show that instabilities associated with vanishing potential-vorticity gradients can develop into stable meanders, eddies or breaking waves. By examining models with different layer depths, we reveal how the dynamics associated with strong-β models qualitatively changes as the strength of the dynamic coupling between the barotropic and baroclinic motions varies.

1. Introduction

Large-scale oceanic fronts are a common phenomenon in the world's oceans. They are formed when differential heating and wind stress act to concentrate isopycnals (see Roden 1975). Fronts can play two important but very different roles depending on their stability. When stable, these fronts are important natural barriers (Cushman-Roisin 1986). They act to hinder both horizontal and vertical motion, restricting the transfer of heat and momentum as well as biological nutrients. On the other hand, fronts can act as a conduit for waves, enhancing along-front transport. Stable fronts also play a role in mid-depth water structure formation, as they force the subduction of cooler waters travelling equatorward, for example, in the Subtropical Convergence Zone of the North Atlantic (Spall 1995). As such, fronts play an important role in determining the structure of the thermocline and general ocean circulation. When

unstable, fronts actually enhance motion as discussed in Karsten & Swaters (2000), the companion article to this paper and hereafter referred to as Part 2.

Large-scale ocean fronts have two principal characteristics. First, ocean surface fronts are largely geostrophic in nature, that is, the velocity is determined, to leading order, by a balance between pressure gradients and the Coriolis effect (Robinson 1983). Second, the variation in isopycnal depth is large, on the scale of the frontal depth itself (Roden 1975). Thus, fronts are characterized by large velocities and the effects of nonlinear advection, particularly in the mass equation, cannot be assumed small. As such, the classic quasi-geostrophic (QG) model, which assumes small isopycnal deflections is not applicable.

There are two ways to overcome this difficulty. The first is to directly analyse the full primitive equations (see, e.g. Griffiths, Killworth & Stern 1982; Killworth 1983; Paldor 1983*a*, *b*; Killworth, Paldor & Stern 1984; Paldor & Killworth 1987; and Paldor & Ghil 1990). Due to the complexity of the primitive equations this approach has several drawbacks. It is often difficult to extend QG analysis to the full primitive equations and fully examine the finite-amplitude regime. The generalization of primitive-equation results to the geometry associated with large-scale open-ocean fronts or to continuously stratified flows is not trivial (see Benilov & Reznik 1996 for a discussion). For example, these models do not include the variation of the Coriolis force with latitude known as the β-effect. Yet, it is known that at large scales the β-effect plays an essential role in determining the evolution of a front (Rhines 1975). While actual ocean fronts often require fully ageostrophic modelling, it is to the benefit of all modellers to examine simple geostrophic limits fully, to assist in the analysis of the more accurate but more mathematically complex semi-geostrophic and fully ageostrophic models (see discussion in Cushman-Roisin 1986).

The second approach is to take advantage of the fact that flows may be geostrophic and have large amplitude if their length scales exceed the Rossby deformation radius (Phillips 1963 and Yamagata 1982). Such motions lie in the 'intermediate scale' between the deformation radius and the planetary scale that is of significant size in the ocean (Charney & Flierl 1981). Yet, it is a common assumption that any complete picture of frontal evolution must involve small scales, those at or shorter than the deformation scale, especially for fronts that outcrop at the surface. However, there are many examples of ocean fronts and motions that do involve scales exceeding the deformation radius (Cushman-Roisin, Sutyrin & Tang 1992; Tang & Cushman-Roisin 1992; and Benilov & Reznik 1996). These include Rossby waves (Chelton & Schlax 1996), mesoscale ocean eddies (Olson *et al.* 1985) and various North Pacific fronts (Roden 1975; Ikeda & Emery 1984; and Ikeda, Emery & Mysak 1984). Recent analysis of TOPEX/POSEIDON data has indicated that ocean eddy energy is concentrated at scales several times the deformation radius (Stammer 1997). As discussed in Part 2, baroclinic waves generally grow at scales greater than the deformation scale with the length scale increasing as they increase in amplitude. Despite the growing evidence of the increasing number and importance of oceanic phenomena that populate the intermediate scale regime, it has not been extensively examined.

Modelling of geostrophic flows larger than the deformation length scale was initially done within the formulation of planetary geostrophic (PG) models (see Williams & Yamagata 1984; de Verdiére 1986; and Pedlosky 1987). Such models, developed for atmospheric dynamics, often emphasized the separation of the planetary scale from the synoptic scale by ignoring the intermediate-scale nonlinear advection terms. However, these terms can be included in a single-layer reduced-gravity model (Williams & Yamagata 1984). Cushman-Roisin (1986) recognized that such a model was well

suited to large-scale ocean fronts that lay in the intermediate-scale regime and included nonlinear advection. This limit was later referred to as the large-amplitude geostrophic (LAG) limit (Benilov 1992, 1993).

Further examination of large-amplitude geostrophic flows within the idealized structure of a layered model has led to the development of two-layer LAG models (see Benilov 1992; Cushman-Roisin *et al.* 1992; Benilov & Reznik 1996; and Karsten & Swaters 1999). The LAG models, as a simple manifestation of an isopycnal model, have the advantage that the vertical resolution is concentrated where the horizontal density gradient is greatest and model surfaces which are the preferred mixing surfaces of the ocean (Chassingnet & Cushman-Roisin 1991). Importantly, the LAG models can be generalized to examine continuously stratified flows (Benilov 1993, 1994) and can incorporate the β-plane approximation (see Karsten & Swaters 1999 for a detailed discussion). As well, LAG models can include outcropping isopycnals that are difficult to examine within the shallow-water equations and impossible within the QG formalism. While there is no doubt that outcropping frontal systems also involve smaller scales, analysis of such outcroppings is incomplete and any insight is valuable.

The LAG models, as simple, rational reductions of the primitive equations, are similar in form to the layered QG model, and thus allow similar analysis. While QG analysis has provided invaluable insight into frontal instabilities, it has also raised many unanswered questions (see Part 2 for a further discussion). The LAG formalism allows further insight into the general dynamics of the shallow-water equations, while emphasizing the effects of large-amplitude isopycnal deflections. As such, it is possible to extend the results of QG analysis, illustrating that the large-amplitude isopycnal formalism can indeed address some of the outstanding issues surrounding QG theory.

Within the formalism of LAG models, there remain two free parameters that allow the possibility of different models: the strength of the β-plane effect and the depth of the frontal layer (see Cushman-Roisin *et al.* 1992; Benilov & Reznik 1996; or Karsten & Swaters 1999 for more details). The strength of the β-plane effect greatly affects the derived model equations and stability characteristics of the described flows. As with QG theory, flows can be separated into two categories based on how the length scale of the motion compares to the Rhines scale,

$$L_{Rhines} = \sqrt{\frac{U_{bt}}{\beta_0}}, \tag{1.1}$$

where U_{bt} is the characteristic barotropic velocity scale and β_0 is the β-plane parameter.

The Rhines scale is the length scale at which β-plane effects balance relative vorticity advection in the barotropic vorticity equation and marks the largest scale to which energy can cascade via baroclinic instability. It acts as a natural dividing scale of the intermediate-length-scale regime (Charney & Flierl 1981). If the length scale of the motion exceeds the Rhines scale the barotropic flow is dominated by β-plane effects and Rossby waves prevail. If the length scale of the motion is less than or equal to the Rhines scale the barotropic flow is governed by the QG evolution of the barotropic relative vorticity and flows are characterized by baroclinic instability.

For the LAG limit, the Rhines scale not only divides motions into large and small scale, but also divides the governing equations into different asymptotic models. Models where the length scale exceeds the Rhines scale are dominated by the β-plane effect and are referred to as strong-β models while those where the length scale is less than or equal to the Rhines scale are called weak-β models (Benilov 1992). In this

paper, we will examine the strong-β models while in Part 2 we examine the weak-β models.

Within both the strong-β and weak-β models, a second important balance exists in the baroclinic motion. This balance is between the coupling of the baroclinic and the barotropic motion and frontal effects, specifically the nonlinear advection associated with the large isopycnal deflection. The strength of the coupling between the baroclinic and the barotropic motion is dependent on the relative depths of the two layers. If the upper, frontal layer is thick, it has a depth similar to that of the lower layer, the flow is strongly coupled and the baroclinic motion is dominated by this coupling. The frontal effects do not contribute to the baroclinic equation to leading order. We will refer to these models as the *thick-upper-layer* models.

As one of the layers (here always assumed to be the upper layer) becomes thinner than the other, the coupling term decreases in size. A critical depth ratio is reached when the baroclinic–barotropic coupling balances the frontal effects and both are included in the baroclinic equation. We will refer to these models as the *thin-upper-layer* models.

If one layer becomes much thinner than the other, the coupling reduces in importance so that it no longer influences the baroclinic motion. The baroclinic motion evolves independent of the barotropic motion and the model is referred to as *decoupled*. Thus, while the focus of this paper is studying the general properties of the strong-β models, it also examines how these properties change as the depth ratio of the layers changes.

In prior works, strong-β models have been derived and analysed using linear approximations (see Benilov & Reznik 1996 for a summary of prior work). The linear analysis has established that isolated fronts with monotonic potential vorticity (PV) profiles are stable when governed by the strong-β models and can support frontally trapped dispersive waves. However, instabilities may occur if the PV gradient vanishes (see Benilov 1995). While linear analysis is always useful, the evolution and effects of fronts depends critically on the nonlinear evolution, especially with intermediate-scale dynamics (Charney & Flierl 1981). Nonlinear interactions modify linear waves, generally increasing their wavelength (Ikeda & Emery 1984 and Ikeda *et al.* 1984). It has been shown that instabilities exist in fronts that have been shown to be linearly stable and are thus attributed to nonlinear effects (Paldor 1987 and Slomp & Swaters 1997). Observations (Barth 1989) and experiments (Griffiths & Linden 1982) have shown that finite-amplitude phenomena such as wave breaking and eddy formation are prevalent in the evolution of fronts. Thus, a full understanding of the evolution of fronts governed by the strong-β dynamics requires a detailed examination of nonlinear effects.

This leads us to the present paper. Here, we extend the previous linear analysis of strong-β models by examining nonlinear effects in these models. We do so by examining the models using both analytical and numerical techniques. We also present the analysis for the decoupled, thin-upper-layer and thick-upper-layer models so as to clearly illustrate the effect of changing the depth ratio. Our goal is to examine three nonlinear effects: how the stable waves are reorganized, how the instabilities associated with vanishing PV gradients evolve and whether any additional nonlinear instabilities are possible.

The plan of this paper is as follows. In § 2, we give a brief derivation of the general strong-β two-layer LAG equations. In § 3 and § 4 we examine the thin-upper-layer and thick-upper-layer models, respectively. The decoupled model is a special case of the thin-upper-layer limit and so is included in the analysis of § 3. In both

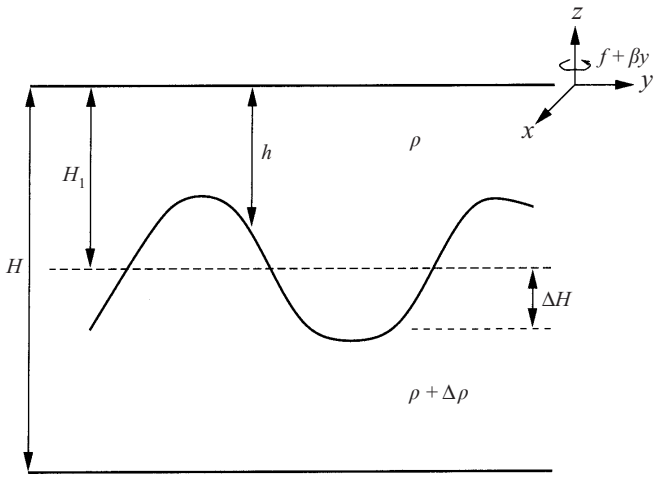

FIGURE 1. The two-layer, rigid-lid, flat-bottom, β-plane model studied in this paper where $h(x, y, t)$ is the dynamic depth of the upper layer, H_1 is the scale of the upper-layer depth, H is the total ocean depth, and ΔH is the scale of the changes in upper-layer depth. The layers are stably stratified with a density difference of $\Delta\rho$.

sections, we begin by presenting the model equations, and a brief review of the linear stability characteristics and solutions. Next, based on the nonlinear invariants, we present a nonlinear stability analysis. Then, using the linear solutions, we present a finite-amplitude analysis that examines the evolution of a slowly varying wave-train under the influence of weak nonlinear effects. In § 5, we analyse the general strong-β model using numerical simulations, concentrating on illustrating the finite-amplitude behaviour and the effect of varying the depth ratio. Finally, in § 6, a summary and the conclusions of the paper as well as comments on future work are presented.

2. Model derivation

The derivation of the general large-amplitude geostrophic model is from the two-layer shallow-water equations in Benilov & Reznik (1996) and, with further discussion and detail, in Karsten & Swaters (1999) (see also Cushman-Roisin *et al.* 1992). The geometry of the flow for a rigid-lid two-layer ocean over a flat bottom is shown in figure 1.

The *general two-layer β-plane LAG equations* are

$$\gamma[\Delta\psi_t + J(\psi, \Delta\psi)] + \beta\psi_x + \mu\nabla\cdot[h(1-\mu\delta h)J(h, \nabla h)] = 0, \tag{2.1}$$

$$h_t + J(\psi, h) - \frac{\varepsilon\beta}{\gamma}h(1-\mu\delta h)h_x - \nu\nabla\cdot[h(1-\mu\delta h)(1-2\mu\delta h)J(h, \nabla h)] = 0, \tag{2.2}$$

where h is the frontal depth and ψ is the barotropic stream function.

The depth ratio, the ratio of the frontal depth, H_1, to the ocean depth H, is broken into two parts, that is,

$$\frac{H_1}{H} = \mu\delta.$$

The parameter δ measures the scale of the ratio; its choice determines the model. The parameter μ is an $O(1)$ parameter that allows variation of the depth ratio within the

chosen model. The parameter β is a similar auxiliary $O(1)$ parameter introduced to explicitly mark the variance of the β-effect after the scaling has been chosen.

The baroclinic velocity scale, U, is given by

$$U = \frac{g' H_1}{f_0 L}$$

giving the baroclinic Rossby number

$$\varepsilon = \frac{U}{f_0 L} = \left(\frac{R_I}{L}\right)^2,$$

where

$$R_I = \frac{\sqrt{g' H_1}}{f},$$

is the internal Rossby deformation radius, with $g' = g\Delta\rho/\rho$ the reduced gravity, and L is the typical length scale of the model. Thus, in this limit, the Burger number and Rossby number are equivalent (see discussion in Cushman-Roisin *et al.* 1992). For geostrophic flow, $\varepsilon \ll 1$, the length scale must exceed the internal deformation radius. Since the Rossby number is the square of the length ratio, a length scale of several times the Rossby deformation is sufficient for a small Rossby number. Critically, this also allows the LAG formalism to examine larger isopycnal slopes than the QG formalism (Benilov 1992). Within the LAG formalism the vertical variations are order $1/\varepsilon$ larger than in the QG formalism while the horizontal length scale is order $1/\sqrt{\varepsilon}$ larger producing isopycnal slopes that are $1/\sqrt{\varepsilon}$ larger.

To ensure that the β-plane plays an important role in the dynamics, the barotropic velocity scale, U_{bt}, is chosen so that the net barotropic advection of the variable planetary vorticity (the β-plane component) scales equivalently to the baroclinic nonlinear advection of upper-layer momentum. That is,

$$H U_{bt} \beta L = H_1 (U_{bc})^2 / L$$

giving that

$$U_{bt} = \frac{H_1}{H}\frac{(U_{bc})^2}{\beta L^2} = \frac{H_1}{H}\left(\frac{R_I}{L}\right)^4 L_\beta f_0, \tag{2.3}$$

where

$$L_\beta = \frac{f_0}{\beta_0}$$

is the planetary length scale. The parameter γ is given by

$$\gamma = \left(\frac{L_{RhLAG}}{L}\right)^6,$$

where

$$L_{RhLAG} = \left(R_I^4 L_\beta^2 \frac{H_1}{H}\right)^{1/6} \tag{2.4}$$

is the LAG Rhines scale found by rearranging (1.1) with the barotropic velocity scale (2.3). The parameter γ compares the length scale of the flow to the Rhines scale and, as such, the strength of the barotropic-relative-vorticity terms to the strength of the β-plane term in the barotropic equation. The Rhines scale (2.4) reflects that within the LAG formalism the appropriate measure of vertical motion is the ratio of frontal

depth to the total ocean depth. For a two-layer QG model the barotropic velocity scale is given by

$$U_{bt} = \frac{g'\Delta H}{f_0 L}$$

where ΔH is the scale of interface deflections. Hence, the Rhines scale (1.1) is given by

$$L_{RhQG} = \left(R_I^2 L_\beta \frac{\Delta H}{H_1} \right)^{1/3} \tag{2.5}$$

(Tang & Cushman-Roisin 1992). Thus, the LAG Rhines scales is smaller than the limit of (2.5) as $\Delta H \to H_1$.

The parameter v, given by

$$v = \frac{\varepsilon}{\sqrt{\delta\gamma}},$$

compares the strength of the nonlinear frontal terms to the strength of the coupling term in the baroclinic equation. Once the strength of the β-effect has been chosen, by choosing the length scale and setting γ, the strength of the coupling is determined by the depth ratio.

In the above discussion, we have assumed that the upper layer is the frontal layer. However, the equations and the geometry are symmetric in the two layers up to a constant in the pressures. As such, the flow of an upper-layer front is identical to the flow of a lower-layer front and equations (2.1) and (2.2) still hold. This is not true when bottom topography is included. Karsten & Swaters (1999) provide a complete discussion of how bottom topography can be included in the general LAG equations.

For the strong-β models $L \gg L_{RhLAG}$ and we set $\gamma = \varepsilon$. This parameter regime implies that the β-effect is included in the leading-order dynamics but the barotropic relative-vorticity terms in (2.1) are an order Rossby number smaller than the β-plane term and can be dropped. Equations (2.1) and (2.2) reduce to

$$\beta\psi_x + \mu\nabla \cdot [h(1 - \mu\delta h)J(h, \nabla h)] = 0, \tag{2.6}$$

$$h_t + J(\psi, h) - \beta h(1 - \mu\delta h)h_x - v\nabla \cdot [h(1 - \mu\delta h)(1 - 2\mu\delta h)J(h, \nabla h)] = 0. \tag{2.7}$$

These are the *general strong-β model equations*. It should be noted that the geometric distortion associated with the β-plane approximation becomes increasingly important at high latitudes. As a result, the strong-β models, as given above, are restricted to mid and low latitudes (see Karsten & Swaters 1999).

Note that when the upper layer vanishes, $h = 0$, the model reduces to the equation

$$\psi_x = 0.$$

This equation does not describe any dynamics at all, but states that, in the absence of the upper layer, the lower-layer flow is any arbitrary zonal flow. This causes difficulty when examining linear solutions across an outcropping where the front vanishes (see § 3.2).

In discussing the stability of the models we will make use of the potential vorticity of each layer. For a layer of fluid governed by the shallow-water equations the potential vorticity, given by,

$$q = \frac{f_0 + \beta_0 y + \nabla \times \boldsymbol{u}}{h},$$

is conserved following the flow. For the strong-β LAG model, we obtain the

expressions

$$q_1 = \frac{1 + (\varepsilon\delta)^{1/2}\beta y + \varepsilon[(1 - \mu\delta h)\Delta h - \mu\delta|\nabla h|^2]}{h} + \text{h.o.t.}, \tag{2.8}$$

$$q_2 = \frac{1 + (\varepsilon\delta)^{1/2}\beta y - \mu\delta\varepsilon[h\Delta h + |\nabla h|^2]}{1 - \mu\delta h} + \text{h.o.t.}, \tag{2.9}$$

for the potential vorticity in the upper and lower layer respectively.

In the open ocean, most large-scale fronts extend across the oceans in the east–west direction between zonal bands of water. This is most easily modelled by a zonally periodic channel given by

$$\Omega = \{(x, y)|x_L < x < x_R,\ -\infty \leqslant W_1 < y < W_2 \leqslant \infty\},$$

where $|W_{1,2}|$ may be very large. The periodicity represents the extended length scale in the east–west direction. The upper, frontal layer is confined to the region $\mathscr{F} \subseteq \Omega$ given by

$$\mathscr{F} = \{(x, y)|x_L < x < x_R,\ W_1 \leqslant \phi_1(x, t) \leqslant y \leqslant \phi_2(x, t) \leqslant W_2\}.$$

When the upper layer does not extend to the walls, that is when $\phi_1 > W_1$ or $\phi_2 < W_2$, the curves $y = \phi_{1,2}(x, t)$ represent the location of the outcroppings where the upper-layer thickness vanishes, i.e. $h = 0$. The curves $\phi_{1,2}$ are, of course, assumed to be periodic in x. As well, we define the domain $\mathscr{NF} = \Omega/\mathscr{F}$ to be the domain where only the lower layer exists, i.e. where $h = 0$.

The boundary conditions on such a domain for a front with a single outcropping at $y = \phi_1$ reduce to (see Karsten 1998 for details)

$$h_x = 0 \quad \text{on} \quad y = W_2, \tag{2.10}$$

$$h|_{y=\phi_1} = 0, \tag{2.11}$$

$$h_t = 0 \quad \text{on} \quad y = W_2, \tag{2.12}$$

$$\psi_x = 0 \quad \text{on} \quad y = W_{1,2}, \tag{2.13}$$

and we require that all dependent variables and all their derivatives are continuous across the periodic boundary $x = x_{L,R}$. If the domain is taken to be infinite in size (2.10) and (2.13) are replaced by

$$|\nabla h|, |\nabla\psi| < \infty \quad \text{as} \quad |y| \to \infty. \tag{2.14}$$

The boundary conditions for other fronts can easily be formulated from those given above.

3. Thin-upper-layer model

3.1. *Model equations*

For the thin-upper-layer model we take the depth ratio to be order Rossby number, that is

$$\delta = \varepsilon \implies \nu = 1. \tag{3.1}$$

The general strong-β model equations (2.6) and (2.7) reduce to

$$\beta\psi_x + \mu J(h, h\Delta h + \tfrac{1}{2}|\nabla h|^2) = 0, \tag{3.2}$$

$$h_t + J(\psi + h\Delta h + \tfrac{1}{2}|\nabla h|^2, h) - \beta h h_x = 0. \tag{3.3}$$

These are the *thin-upper-layer model equations.*

One can eliminate the nonlinear frontal terms in (3.3) by forming (3.2) $-\mu$ (3.3) to get

$$\mu h_t + J(\psi, \mu h + \beta y) - \mu\beta h h_x = 0. \tag{3.4}$$

Equation (3.3) governs the upper-layer dynamics while (3.4) governs the lower-layer dynamics. Considering only (3.3) in the limit as $\psi \to 0$ gives the decoupled (or reduced-gravity) model first established in Williams & Yamagata (1984) and examined in Cushman-Roisin (1986). It is also referred to as the PG equation.

The PV for each layer is found by substituting (3.1) into (2.8) and (2.9) giving

$$q_1 = \frac{1}{h} + \varepsilon\frac{\Delta h + \beta y}{h} + O(\varepsilon^2), \tag{3.5}$$

$$q_2 = 1 + \varepsilon(\mu h + \beta y) + O(\varepsilon^2). \tag{3.6}$$

Note that the barotropic stream function does not appear in the leading-order potential vorticities indicating that this model is dominated by baroclinic and β-plane dynamics.

To analyse the model equations, we need a basic-state flow that is a solution to the full nonlinear model. From (3.2) and (3.3) it follows that any zonal flow, where the model variables are allowed to vary in the meridional direction only, is a solution to the fully nonlinear model. In principle, most of the following analysis can be carried out with barotropic flows present. However, their effect is not of great interest in these inherently baroclinic models and we take the basic-state barotropic flow to be quiescent. Hereafter, we will indicate the basic-state zonal flow with a subscript zero, that is, $h_0(y)$.

3.2. *Linear analysis*

In this paper, we will be looking at nonlinear interactions. But in order to do so, it is necessary to understand the linear stability and calculate linear solutions. The linear equations are found by setting the model variables to be the sum of the basic state and some perturbation, that is

$$\left.\begin{aligned} h(x,y,t) &= h_0(y) + \tilde{h}(y)\exp[\mathrm{i}(kx-\omega t)] + \text{c.c.},\\ \psi(x,y,t) &= \psi_0(y) + \tilde{\psi}(y)\exp[\mathrm{i}(kx-\omega t)] + \text{c.c.},\\ \phi(x,y,t) &= \phi_0 + \tilde{\phi}(y)\exp[\mathrm{i}(kx-\omega t)] + \text{c.c.}, \end{aligned}\right\} \tag{3.7}$$

where the basic flow has an outcropping at $y = \phi_0$, that is

$$h_0(\phi_0) = 0,$$

and $k \geqslant 0$ is the along-front wavenumber, $\omega = \omega_R + \mathrm{i}\omega_I$ is the complex-valued frequency, and c.c. stands for complex conjugate. The phase speed of the wave is given by $c = \omega/k$.

The linear travelling-wave or normal-mode equations are found by substituting (3.7) into (3.2) and (3.3) giving, after some reorganization,

$$(\mu h_0' + \beta)[h_0(h_0'\tilde{h}' - h_0''\tilde{h})]' - [(\mu h_0' + \beta)h_0 h_0' k^2 + \beta(\beta h_0 + c)]\tilde{h} = 0, \tag{3.8}$$

$$\tilde{\psi} = \frac{\mu}{\beta + \mu\alpha}(c + \beta h_0)\tilde{h}. \tag{3.9}$$

The boundary conditions are the linearized versions of (2.10)–(2.14).

At an outcropping, it is necessary to impose continuity conditions on the barotropic stream function. Usually, see for example, Swaters (1993*a*, *b*) or Swaters (1991), these reduce to the condition that the lower-layer pressure is continuously differentiable across the outcropping. Since the model does not describe motion in the absence of an upper layer, imposing such a condition would eliminate all possible wave motion at the outcropping. This is a grave limitation of the linear analysis of this model. By definition, an outcropping where h_0 vanishes must be governed by small-scale (cross-frontal) nonlinear dynamics. Therefore, we assume that the outcropping constitutes a nonlinear boundary layer that allows the linear solution to be smoothly matched to the non-frontal, no-wave-motion region. This solution must be considered with the proper amount of discretion. It is useful nevertheless to present the analysis for another reason. In the limit as $\psi \to 0$, the analysis can be applied to the decoupled model which, with no motion in the lower layer, requires no matching conditions. As such, the finite-amplitude analysis that follows extends the f-plane analysis of Slomp & Swaters (1997) to a β-plane.

In Benilov & Cushman-Roisin (1994), the stability of the linear model (3.8), (3.9) was examined. It was argued that if

$$\frac{\beta h_0'}{\mu h_0' + \beta} \tag{3.10}$$

has the same sign for all $y \in [\phi_{10}, W_2]$ then $\omega_I = 0$ for all wavenumbers. It follows that instability can only occur if $h_0' = 0$ or $h_0' = -\beta/\mu$ for some value of y. These two points are singular points of (3.8) and correspond to points where the leading-order PV gradients vanish (see (3.5) and (3.6)). This is a much stronger necessary condition for instability than in a QG model where if the PV gradient reverses sign across the layer interface, instability is possible.

The manner in which instability arises when these singularities exist in the basic flow is discussed in Benilov (1995). These instabilities are of vital importance in the evolution of the front as they provide the only source for linear growth. However, analysis of the linear problem near the singularities is understandably complex. While the singularities can be regularized, solutions can only be obtained through numerical integration of the linear equations (see Benilov 1995). As a result, the linear solutions presented below, and the finite-amplitude analysis based on these solutions are only valid for flows without these singularities. On the other hand, the nonlinear stability analysis and the numerical solutions do allow analysis of the singular points. As such, we will provide a greater discussion of these singular points in these frameworks.

We will discuss linear solutions for linearly sloping fronts. More complicated frontal profiles can be examined numerically and the results are qualitatively similar. For a gently sloping front we take

$$h_0(y) = 1 + \alpha \left(y - \frac{W_2 - W_1}{2} \right), \quad W_1 \leqslant y \leqslant W_2, \tag{3.11}$$

where the parameters are chosen such that $h_0 > 0 \; \forall \; y$, that is, the front extends across the entire channel. In order to obtain an interesting analytic solution, we assume that the model parameters are small, that is

$$\alpha = \Delta\tilde{\alpha}, \; \beta = \Delta\tilde{\beta}, \; \omega = \Delta\tilde{\omega}, \; c = \Delta\tilde{c}, \tag{3.12}$$

where $0 < \Delta \ll 1$ and $\tilde{\alpha}$, $\tilde{\beta}$, $\tilde{\omega}$ and $\tilde{c}$ are $O(1)$ parameters. (The rescaling of the frequency and phase velocity is equivalent to rescaling the time scale to a longer scale.) These rescalings allow us to examine what is essentially a QG flow, with

small-amplitude deflections in the interface, but at the longer time and larger length scales of the LAG model.

To leading order in Δ, (3.8) reduces to

$$\tilde{\alpha}(\mu\tilde{\alpha}+\tilde{\beta})(\tilde{h}''-k^2\tilde{h})-\tilde{\beta}(\tilde{\beta}+\tilde{c})\tilde{h}=0.$$

The solutions are sinusoids leading to the dispersion relationship

$$\tilde{c}(k,\ell)=-\left[\tilde{\beta}+\frac{\tilde{\alpha}(\mu\tilde{\alpha}+\tilde{\beta})(k^2+\ell^2)}{\tilde{\beta}}\right], \tag{3.13}$$

where ℓ is the meridional wavenumber.

Benilov & Cushman-Roisin (1994) also found that a solution to the model could be found for a wedge-like front given by

$$h_0(y)=\begin{cases}\alpha y, & \alpha y\geqslant 0,\\ 0, & \alpha y<0,\end{cases} \tag{3.14}$$

corresponding to a constant baroclinic flow with no barotropic flow. The solution is an extension of the linear solution found in Cushman-Roisin (1986) for the decoupled model and the wedge front (3.14). Again, it should be recognized that the solution below for the wedge front does not meet the condition that the leading-order barotropic stream function be smooth across the outcropping. Its validity, presumably, is based on the assumption explained previously.

With the wedge profile (3.14) the normal-mode equation (3.8) reduces to

$$y\tilde{h}''+\tilde{h}'-[(\alpha\kappa(k))^2y+\hat{c}]\tilde{h}=0, \tag{3.15}$$

where

$$\kappa(k)=\sqrt{\frac{k^2}{\alpha^2}+\frac{\hat{\beta}\beta}{\alpha^3}},\quad \hat{c}=\frac{\hat{\beta}c}{\alpha^2},\quad \hat{\beta}=\frac{\beta}{\mu\alpha+\beta}. \tag{3.16}$$

When κ is real, the solution to (3.15) that satisfies the boundary conditions is

$$\tilde{h}(y,k,n)=A\exp(-\alpha\kappa(k)y)L_n(2\alpha\kappa(k)y), \tag{3.17}$$

where L_n is the Laguerre polynomial of degree $n\geqslant 0$, with the corresponding dispersion relationship

$$c(k,n)=-\frac{\alpha^3\kappa(k)(2n+1)}{\hat{\beta}} \tag{3.18}$$

(see Cushman-Roisin 1986 for details). For imaginary κ, a continuous spectrum of stable travelling waves is realized (see Cushman-Roisin 1986 for details). This solution is not suitable for further analysis and is not discussed in detail.

For both linear solutions, it should be noted that in the special case where $\beta=0$ the model becomes degenerate and wave solutions are not possible. There are no longer any terms related to time derivatives, and thus the frequency ω, and, as a result, no dispersion relationship for ω exists. Physically, without the β-plane effect there is no mechanism to generate barotropic waves.

The reduced-gravity limit for both fronts is obtained by letting μ tend to zero. In this limit, waves that travel against the basic-state flow are not possible. For the wedge model, the results of Cushman-Roisin (1986) are obtained. It should be noted that in the single-layer model with $\beta=0$ travelling-wave solutions are still possible (see Slomp & Swaters 1997).

3.3. *Nonlinear invariants and a stability theorem*

In Cushman-Roisin *et al.* (1992) it was noted that the pseudo-energy

$$\mathscr{E} = \frac{1}{2}\iint_{\mathscr{F}} h\nabla h \cdot \nabla h - \beta y h^2 \,\mathrm{d}x\,\mathrm{d}y \tag{3.19}$$

is conserved by the thin-upper-layer model (3.2) and (3.3). Demonstrating that this quantity is invariant can be accomplished by using the governing equations and the boundary conditions or as a consequence of energy and PV conservation of the shallow water equations (Karsten 1998). The first term in $\mathscr{E}$ is the baroclinic kinetic energy, the second is associated with the β-effect. The fact that $\mathscr{E}$ is conserved means that any increase in the baroclinic kinetic energy must be accompanied by a northward movement of upper-layer fluid.

We also have invariants associated with the leading order PVs, namely

$$\mathfrak{C}_1(h) = \iint_{\mathscr{F}} \Phi_1(h)\,\mathrm{d}x\,\mathrm{d}y, \tag{3.20}$$

$$\mathfrak{C}_2(h) = \iint_{\Omega} \Phi_2(\mu h + \beta y)\,\mathrm{d}x\,\mathrm{d}y, \tag{3.21}$$

where $\Phi_{1,2}$ are arbitrary, sufficiently smooth function of their arguments. The similarity of the invariants (3.20) and (3.21) allows us to construct another invariant, given by

$$\mathfrak{M} = \iint_{\mathscr{F}} yh\,\mathrm{d}x\,\mathrm{d}y. \tag{3.22}$$

Equation (3.22) is the upper-layer zonal momentum invariant (see Slomp & Swaters 1997). It should be noted that (3.19), (3.20), and (3.22) are also invariants of the decoupled model stressing the similarity of the thin-upper-layer model and the decoupled model.

Since none of the above invariants involve the barotropic stream function, it is not possible to use them to establish stability theorems that bound a perturbation norm involving the barotropic stream function. We can, however, find conditions on a zonal flow that establish nonlinear bounds on the perturbation upper-layer depth only. Establishing such bounds often involves a constrained zonal momentum invariant, i.e. the zonal momentum invariant plus the leading-order PV invariant (see Slomp & Swaters 1997 or Karsten & Swaters 1996). But, since the zonal momentum invariant is a linear combination of the two PV invariants, the analysis can be carried out using only the PV invariants. As in Slomp & Swaters (1997) and Karsten & Swaters (1996), we only examine a basic-state front that extends across the entire domain and does not outcrop. (The stability argument breaks down when an outcropping occurs because we are unable to bound the finite variations of the outcropping without additional assumptions.)

The stability conditions are determined by considering

$$\mathfrak{I}(\tilde{h} + h_0) = \mathfrak{C}_1(\tilde{h} + h_0) - \mathfrak{C}_1(h_0) + \mathfrak{C}_2(\tilde{h} + h_0) - \mathfrak{C}_2(h_0)$$

where $h_0 = h_0(y)$ represents a basic-state zonal flow, $\tilde{h}$ is the perturbation to this flow, and $\mathfrak{C}_1$ and $\mathfrak{C}_2$ are given by (3.20) and (3.21), respectively, with the domains of integration extended to the entire domain Ω. Obviously, $\mathfrak{I}(h)$ is an invariant of the flow since $\mathfrak{C}_1(h)$ and $\mathfrak{C}_2(h)$ are. The following nonlinear stability result holds:

THEOREM 3.1. *The zonal flow $h_0(y)$ is nonlinearly stable in the sense of Liapunov with respect to the perturbation norm*

$$\|\tilde{h}\|^2 = \iint_{\Omega} \tilde{h}^2 \,\mathrm{d}x\,\mathrm{d}y, \tag{3.23}$$

if there exist real constants A and B such that either

$$0 < A \leqslant \Phi_1''(\xi) + \mu^2 \Phi_2''(\mu\xi + \beta y) \leqslant B < \infty, \tag{3.24}$$

or

$$-\infty < B \leqslant \Phi_1''(\xi) + \mu^2 \Phi_2''(\mu\xi + \beta y) \leqslant A < 0, \tag{3.25}$$

for all $\xi \geqslant 0$ and $y \in [W_1, W_2]$, where

$$\Phi_1'(h_0) + \mu \Phi_2'(\mu h_0 + \beta y) = 0, \tag{3.26}$$

for all $y \in [W_1, W_2]$.

Equation (3.26) establishes that the first variation of $\mathfrak{I}$ vanishes and, thus, that $\mathfrak{I}$ is quadratic in the perturbations. The conditions (3.24) and (3.25) establish that $\mathfrak{I}$ is either positive or negative definite, respectively, and it follows accordingly (see Karsten 1998) that

$$\|\tilde{h}\|^2 \leqslant \frac{B}{A} \|\tilde{h}(t=0)\|^2 \quad \forall\ t,$$

establishing Liapunov stability. It should be noted that we have only bounded the perturbations in h in this theorem and have not considered whether ψ could become unbounded. However, it is growth in h that represents *baroclinic* instability, that is, changes in the frontal structure releasing available potential energy.

Before interpreting the nonlinear stability conditions, we discuss the connection of this analysis to the linear stability conditions of the previous section. Linear stability conditions can also be established if (3.26) holds and the second variation of $\mathfrak{I}$ evaluated at $\tilde{h} = 0$, hereafter $\delta^2\mathfrak{I}(h_0)$, is definite and conserved by the linear equations. If (3.24) or (3.25) holds for all $\xi = h_0(y)$, then $\delta^2\mathfrak{I}(h_0)$ is definite. However, $\delta^2\mathfrak{I}(h_0)$ is not trivially conserved by the linear equations as it is for the decoupled model (see Slomp 1995). In order to establish that $\delta^2\mathfrak{I}(h_0)$ is conserved by the linear equations, it is required that

$$\frac{\mathrm{d}^2}{\mathrm{d}y^2}\Phi_1'(h_0) = \frac{\mathrm{d}^2}{\mathrm{d}y^2}\Phi_2'(\mu h_0 + \beta y) = 0,\ \forall\ y \in [W_1, W_2]. \tag{3.27}$$

Conditions (3.26) and (3.27) imply that

$$\Phi_1''(h_0) + \mu^2 \Phi_2''(\mu h_0 + \beta y) = \frac{C\beta}{h_0'(\mu h_0' + \beta)}$$

for some arbitrary constant C. Thus, (3.24) or (3.25) can hold for all $\xi = h_0(y)$ only if $h_0'(\mu h_0' + \beta) \neq 0\ \forall\ y \in [W_1, W_2]$. Therefore, all fronts which do not contain either of the PV singular points are linearly stable. This result extends the stability theorem of Benilov & Cushman-Roisin (1994) to all forms of perturbations, not only wave-like perturbations.

In order to interpret and apply the nonlinear stability results we return to the analysis given in Slomp & Swaters (1997). Consider choosing the PV invariants so that $\mathfrak{I}$ is the momentum invariant constrained by the upper-layer PV invariant,

that is

$$\mathfrak{J}(\tilde{h}+h_0) = \mathfrak{M}(\tilde{h}+h_0) - \mathfrak{M}(h_0) - \mathfrak{C}_1(\tilde{h}+h_0) + \mathfrak{C}_1(h_0)$$
$$= \iint_\Omega y\tilde{h} - \Phi_1(\tilde{h}+h_0) + \Phi_1(h_0)\,\mathrm{d}x\,\mathrm{d}y, \tag{3.28}$$

where Φ_1 remains arbitrary and we have chosen the negative sign for simplicity. Condition (3.26) implies $\Phi_1'(h_0) = y$, that is, Φ_1' is the inverse of h_0. We define $h_0^+(y)$ as the smooth extension of $h_0(y)$ so that $\Phi_1'(\xi) = \Phi_1'(h_0^+(y)) = y$ is defined for all $\xi \geqslant 0$. Then, (3.24) or (3.25) is satisfied if

$$0 < \left|\frac{\mathrm{d}h_0^+}{\mathrm{d}y}\right| < \infty. \tag{3.29}$$

For smooth fronts, $h_0' \neq 0\ \forall\ y \in [W_1, W_2]$ is sufficient to construct h_0^+ such that (3.29) is satisfied. It follows that all smooth, strictly monotonic fronts are nonlinearly stable. The above result holds for the decoupled model as well and thus extends the result of Slomp & Swaters (1997) to the decoupled model on the β-plane.

For the thin-upper-layer model, we can also consider the invariant formed by constraining the momentum invariant by the lower-layer PV invariant, that is

$$\mathfrak{J}(\tilde{h}+h_0) = \mathfrak{M}(\tilde{h}+h_0) - \mathfrak{M}(h_0) - \mathfrak{C}_2(\tilde{h}+h_0) + \mathfrak{C}_2(h_0)$$
$$= \iint_\Omega y\tilde{h} - \Phi_2(\mu\tilde{h} + \mu h_0 + \beta y) + \Phi_2(\mu h_0 + \beta y)\,\mathrm{d}x\,\mathrm{d}y, \tag{3.30}$$

where Φ_2 remains arbitrary. Condition (3.26) implies $\Phi_2'(\mu h_0 + \beta y) = y$, that is Φ_2' is the inverse of $\mu h_0 + \beta y$. Now let $h_0^+(y)$ be the smooth extension of $h_0(y)$ so that $\Phi_2'(\xi) = \Phi_2'(\mu h_0^+ + \beta y) = y$ is defined for all $\xi \geqslant \beta W_1$. (Note that ξ must take on all possible values of $\mu h + \beta y$ for $h \geqslant 0$ and $y \in [W_1, W_2]$.) Then, (3.24) or (3.25) is satisfied if

$$0 < \left|\frac{\mathrm{d}h_0^+}{\mathrm{d}y} + \beta\right| < \infty. \tag{3.31}$$

For smooth fronts, $\mu h_0' + \beta \neq 0\ \forall\ y \in [W_1, W_2]$ is sufficient to construct h_0^+ such (3.31) is satisfied. It follows that all smooth fronts where $\mu h_0' + \beta \neq 0$ are nonlinearly stable. Therefore, all sufficiently smooth fronts are nonlinearly stable unless both of the singular points occur in the domain. When both singular points exist, the interaction of the two growing waves may allow for the unstable growth to finite size independent of the initial disturbance amplitude.

This result is somewhat puzzling in the light of the linear results. Benilov (1995) established that each singular point alone is a possible source of linear growth. However, the above analysis states that these instabilities cannot exist in the full nonlinear model. This dichotomy between the linear and nonlinear models was suggested in the above discussion where the development of a linear theory requires additional constraints to establish the conservation of the linearized invariant.

This discussion raises the question of what stability results should be expected in numerical simulations and oceanic observations of such fronts. To consider such cases, we must consider how smaller scale motions and dissipation will affect the given theorems. It should be noted that the linear instability results can be derived by adding dissipation to the model and considering the limit of vanishing viscosity (see Benilov 1995). On the other hand, the nonlinear results depend crucially on the exact conservation of the nonlinear invariants. When smaller scales or dissipation

enter into the model, these nonlinear invariants are no longer conserved. It is not a trivial matter to determine how the conservation of the PV invariants is affected by dissipation. Thus, one may conclude that the linear instability may be more physical than the ideal nonlinear stability result. In § 5.2 we examine numerical simulations of these models which demonstrate that the linear instability does exist with a single PV singularity, despite the nonlinear result.

3.4. *Finite-amplitude analysis*

In this subsection, the effects of the nonlinear terms in the model are examined. We begin by examining the envelope equation governing the finite time and space evolution of the amplitude of a given wave-train. This analysis naturally leads to a discussion of resonances and we include a discussion of long-wave–short-wave resonance. The method we use to derive a finite-amplitude equation governing the evolution of a slowly-varying wave amplitude follows that of Newell (1974) and Grimshaw (1977), and is similar to the analysis of the decoupled model studied in Slomp (1995) and Slomp & Swaters (1997). In this paper, we will present only selected details of the analysis. The remaining details, including lengthy derivations, are fully described in Karsten (1998).

We assume we have a basic state with a wave-like perturbation of amplitude Δ, that is

$$\left.\begin{aligned} h &= h_0 + \Delta\{A(X,T,\tau)\tilde{h}(y)\exp[\mathrm{i}(kx-\omega t)] + \text{c.c.}\} + O(\Delta^2), \\ \psi &= \Delta\{A(X,T,\tau)\tilde{\psi}(y)\exp[\mathrm{i}(kx-\omega t)] + \text{c.c.}\} + O(\Delta^2), \end{aligned}\right\}$$

where $A(X,T,\tau)$ is the slowly-varying wave amplitude, $T = \Delta\tilde{t}$, $\tau = \Delta^2\tilde{t}$, $X = \Delta x$ are slow space and time variables introduced to examine the space and time scales associated with nonlinear interaction of the fundamental mode. Inserting such a solution into the model equations (3.2) and (3.3) and setting the coefficients of terms of similar orders in Δ to zero gives a series of problems that must be solved. The solvability conditions that arise at each order finally determine an evolution equation for the wave amplitude A.

The leading-order problem is the linear problem for the given basic state as discussed in § 3.2. For the next order problem, an asymptotically consistent solution can only be found provided

$$A_T + \frac{\partial\omega}{\partial k}A_X = 0.$$

This is the simple statement that to this order the wave amplitude, and thus the wave energy, travels at the group velocity, $c_G = \partial\omega/\partial k$ and we introduce $\xi = X - c_G T$. Finally, from the third-order problem we find that A satisfies the nonlinear Schrödinger equation (NLS)

$$\mathrm{i}A_\tau + \lambda A_{\xi\xi} = N|A|^2 A \tag{3.32}$$

where $\lambda = (1/2)\partial^2\omega/\partial k^2$ and N measures the nonlinear interactions.

The NLS equation can be examined in many ways (see Newell 1974; Craik 1985; and Slomp 1995). Of greatest interest to us here is the development of Benjamin–Feir (hereafter BF) or sideband instability. If BF instability occurs, initial perturbations can reorganize themselves into travelling-wave or soliton solutions with a larger length scale and greater amplitude than the initial perturbations. The equation is separated into two qualitative classes of solutions based upon the sign of the ratio $\Gamma_1 = N/\lambda$ (see Craik 1985). If $\Gamma_1 < 0$, the wave-train is subject to BF instability; if $\Gamma_1 > 0$, the

wave-train is stable. It would appear that the possibility of instability would violate the nonlinear stability theorem established in § 3.3. However, as discussed in Newell (1974) and Slomp & Swaters (1997), this instability reorganizes the neutral modes into travelling-wave packets/soliton solutions whose amplitude is bounded by the initial state and therefore remain nonlinearly stable. If the wave-train is subject to BF instability a 'bright' soliton can form, if not, a 'dark' soliton solution is possible.

For the gently sloping front (3.11), it follows, with proper considerations of the rescaled variables and wave amplitude, that

$$\Gamma_1 = -\frac{k^2\ell^2[k^2(1+\eta+\eta^2) - 3\ell^2(1+3\eta+3\eta^2)]}{9\alpha^2(1+\eta)^2(k^2-\ell^2)}, \tag{3.33}$$

where $\eta = \mu\alpha/\beta$ (see Karsten 1998 for details). Hence, $\Gamma_1 < 0$, and the wave is subject to BF instability when the waves have a relatively large zonal scale, $k < \ell$, or a relatively small zonal scale $k > k_c$ where

$$k_c^2 = \ell^2\left[\frac{3(1+3\eta+3\eta^2)}{1+\eta+\eta^2}\right]. \tag{3.34}$$

The growth rate associated with the BF instability is proportional to Γ_1 and grows as k increases. Thus, the smallest scales experience a rapidly growing instability and are quickly reorganized into larger-scale structures. This leads to a cascade of energy from the smallest scales to larger-scale structures.

The solution breaks down when $k = \ell$, where a long-wave–short-wave (hereafter LWSW) resonance occurs (see Karsten 1998). The LWSW resonance occurs when a long-wave solution to the leading-order slow problem has a phase speed and group velocity equal to that of the group velocity of the fundamental, short-wave solution. That is,

$$c_G(0,m) = c(0,m) = c_G(k,\ell), \tag{3.35}$$

where m is the meridional-mode wavenumber of the long wave.

In order to examine the effects of LWSW resonance, a long-wave solution must be included in the analysis from the beginning. We assume that the perturbation is composed of two parts: a fast varying or short wave analogous to the perturbation of the previous analysis and a slowly-varying or long wave independent of the fast variables x and t, that is

$$\left.\begin{aligned} h &= h_0 + \Delta\{A(X,T,\tau)\tilde{h}(y,k,l)\exp[\mathrm{i}(kx-\omega t)] + \text{c.c.}\} \\ &\quad + \Delta^{4/3}B(X,T,\tau)\tilde{h}(y,0,m) + O(\Delta^{5/3}), \\ \psi &= \Delta\{A(X,T,\tau)\tilde{\psi}(y,k,l))\exp[\mathrm{i}(kx-\omega t)] + \text{c.c.}\} \\ &\quad + \Delta^{2/3}B(X,T,\tau)\tilde{\psi}(y,0,m) + O(\Delta^{5/3}), \end{aligned}\right\} \tag{3.36}$$

where $A(X,T,\tau)$ is the short-wave amplitude, $B(X,T,\tau)$ is the long-wave amplitude, and $T = \Delta^{2/3}\tilde{t}$, $\tau = \Delta^{4/3}\tilde{t}$, $X = \Delta^{2/3}x$ are new slow space and time variables. The scales and amplitudes are chosen so that we get the desired balance (see Grimshaw 1977 or Karsten 1998 for details).

We also allow for near resonance, that is, we choose

$$c_G(k,\ell) = c_G(0,m) + \Delta^{4/3}\zeta, \tag{3.37}$$

where ζ is an $O(1)$ tuning parameter that specifies how close to exact resonance, $\zeta = 0$, we are. Since relatively large variations in the wavenumber result in only a

small values of the tuning parameter, the following results are relevant to a wide range of wavenumbers.

Once again, by substituting (3.36) into (3.2), (3.3) and considering terms of similar orders in Δ, we obtain a series of problems that must be solved. At $O(\Delta)$ the linear solution is obtained for the short wave. At $O(\Delta^{4/3})$, the long wave trivially satisfies the linear equations. At $O(\Delta^{5/3})$, the second-order solution for the short wave is obtained, with the stipulation that the amplitude travels at the group velocity, $A = A(\xi, \tau)$. At $O(\Delta^2)$, the linear long-wave equation with the appropriate resonant solution is found.

At $O(\Delta^{7/3})$, the second-order, slow derivatives of A, as given in (3.32), are balanced by the leading-order interaction of the short and long waves. At $O(\Delta^{8/3})$, the slow-time derivative of $\tilde{B}$ and the tuning error term are balanced by the slow, quadratic interactions of the short wave with itself. These final two balances give the LWSW equations derived by Grimshaw (1977) and Djordjevic & Redekopp (1977) and studied by Ma (1978). They can be written in the normalized form

$$\mathrm{i}A_\tau + \lambda A_{\xi\xi} = AB, \tag{3.38}$$

$$B_\tau = \zeta B_\xi + \Gamma_2(|A|^2)_\xi, \tag{3.39}$$

where $\lambda = (1/2)\partial^2\omega/\partial k^2$ (see Karsten 1998 for details).

Examining the stability of the Stokes wave solution with amplitude a_0, yields the dispersion relationship

$$\sigma^3 - \zeta\Re\sigma^2 - \lambda^2\Re^4\sigma + 2\Gamma_2\lambda a_0^2\Re^3 + \lambda^2\zeta\Re^5 = 0. \tag{3.40}$$

If (3.40) has complex roots then the wave-train is unstable, and the LWSW equations have a BF instability similar to that discussed earlier. Such an instability indicates that energy is being transferred from the short wave to the long wave. The instability is inhibited if the tuning is positive and shifted to smaller scales if the tuning is negative.

For the gently sloping front profile (3.11), we have (see Karsten 1998)

$$\Gamma_2 = -2(1+2\eta)^2k^3\ell^2(3\ell^2 - k^2),$$

and the characteristics of the instability can be determined straightforwardly by solving the dispersion relationship (3.40). In order to compare the growth rates associated with the LWSW resonance with that of the BF instability, we must scale them appropriately using the new slow time scaling. For example, choosing $\Delta = 0.1$, we can combine the results for the LWSW resonance with the BF instability. We assume that the LWSW resonance dominates the flow for $k < k_c$ and that BF instability applies for $k > k_c$ where k_c is given by (3.34).

In figure 2, we plot the maximum growth rate in the $(\eta, k/\ell)$-plane. The graph is symmetrical about $\eta = -1$ and the region of stability is quite small. Within the region $-1 < \eta < 0$, where the phase velocity can be negative, the wave-train is more susceptible to unstable growth. The growth rates at small scales are significant and are a result of the LWSW resonance. At large wavenumbers (small wavelengths) the growth rate of the BF instability becomes comparable to and eventually exceeds the growth rate associated with the LWSW resonance.

The above analysis can be repeated for the wedge front profile (3.14). The parameters $\Gamma_{1,2}$ cannot be obtained analytically but can be calculated numerically by expanding the nonlinear terms (see Karsten 1998). Once again, Γ_1 can take on both negative and positive values depending on complex relationships of the wavenumbers and other parameters. The analysis becomes more complex as the front allows an

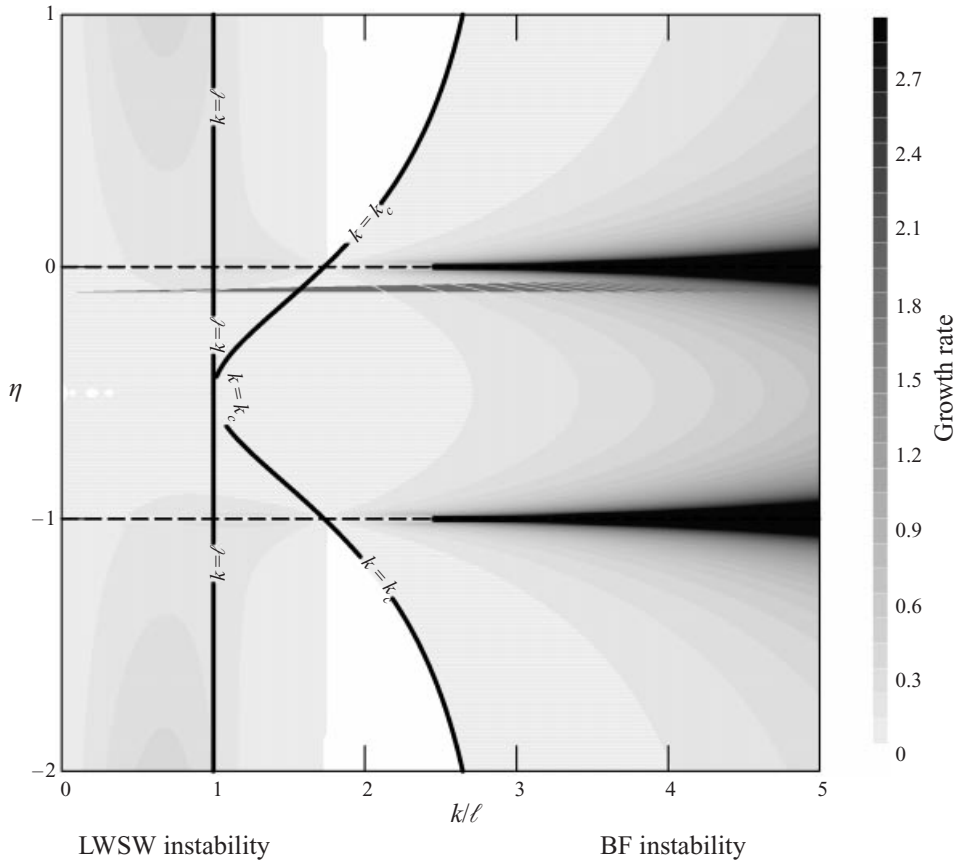

FIGURE 2. The maximum growth rate when the effects of both the LWSW resonance and BF instabilities are considered for the thin-upper-layer model, gently sloping front analysis. White regions are stable while darker grey indicates higher growth rates as shown on the scale on the right. The dashed lines mark the PV singularities and the solid lines mark the critical values of k.

infinite number of long waves to resonate with the fundamental mode (see Karsten 1998). For each of these LWSW resonances, an instability grows which transfers energy to the long wave.

In figure 3, the maximum growth rates as determined by the BF instability and the LWSW instability are plotted versus k^2 for $\eta = \frac{1}{2}$. Now, the LWSW resonance dominates the BF instability giving unstable growth for all wavenumbers. The possibility of several resonances complicates the picture, as the instabilities associated with different resonant modes overlap. Thus, it becomes unclear which instability will dominate the evolution, although it is clear that growth rates increase as the wavelength decreases and that all wavenumbers are subject to unstable growth. The growth rates associated with these instabilities are an $O(\Delta)$ larger than those associated with the gently sloping front and increase as the frontal slope increases. We conclude that increasing the slope of the front, and hence the amplitude of the zonal flow, enhances the energy cascade to the larger scales associated with the envelope variations and long waves. Such an energy cascade, especially through the LWSW resonance, may lead to the development of zonal jets.

For both fronts, we can examine the decoupled limit by taking the limit $\mu \to 0$. For

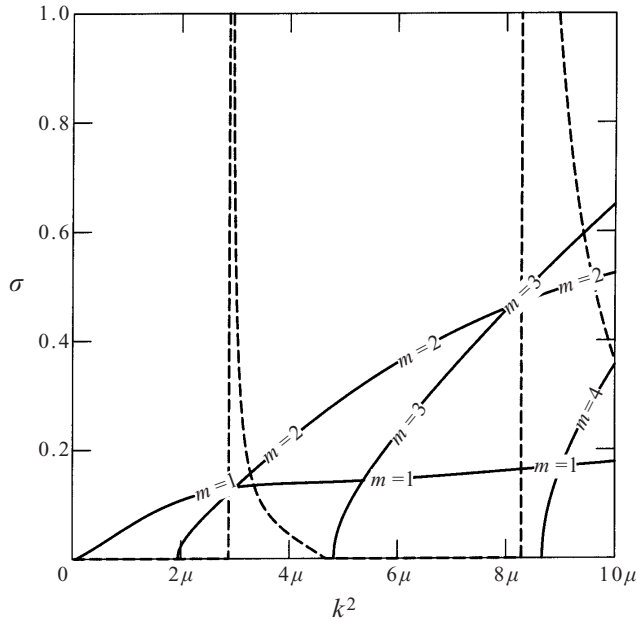

FIGURE 3. The growth rates of the BF instability (dashed line) and the LWSW resonance (solid line) for the thin-upper-layer model, wedge front analysis. The LWSW lines are labeled with the long-wave mode they correspond to.

the gently sloping front, the results are now symmetrical for eastward and westward flows. For the wedge front the results are qualitatively the same with the LWSW resonance dominating. We can conclude that the addition of the lower layer does not have a dramatic influence on the nonlinear effects in the strong-β limit. However, no resonances occurred in the decoupled model on an f-plane (see Slomp & Swaters 1997). Thus, the inclusion of the β-plane terms in the model does lead to an essential difference in the nonlinear evolution of the flow. We can also examine the limit as the model tends towards a thick upper layer, $\mu \to \infty$. Once again the results are now symmetrical for eastern and western flows.

It should be noted that other finite-amplitude analyses can be done. For example, three-wave interactions can be examined. In Karsten (1998), it is shown that triads of resonance waves exist for both fronts. These resonances result in a periodic exchange of energy between the waves with no clear preference in scale. As such, they act simply to redistribute energy to all scales. As well, Karsten (1998) showed that very long waves may break due to the hyperbolic nature of the governing equations when large scales are considered (see Anderson & Killworth 1979 and Dewar 1987 for a discussion of similar planetary shock waves in the decoupled model).

4. Thick-upper-layer model

We now discuss the thick-upper-layer model first derived and examined in Benilov (1992). Much of the analysis presented is similar to that of § 3 and so we will be quite brief. The thick-upper-layer model does provide important insight into increasing the coupling between the baroclinic and barotropic modes while removing the restriction of a thin upper layer. However, this comes at the cost of requiring a large length scale, often so large that spherical coordinates may be required as the geometric distortion

associated with the Earth's curvature is no longer small (see Karsten & Swaters 1999 for a complete discussion). As well, the model can be described only in the context of baroclinic/barotropic flow and not as a layer model *vis-á-vis* Cushman-Roisin *et al.* (1992). This reflects the fact that the model describes the motion of the two layers equally and not of an active layer coupled to a more passive layer.

4.1. *Model equations*

The thick-upper-layer model corresponds to a scaling where the depth ratio is $O(1)$ and we set

$$\delta = 1, \quad \nu = 0. \tag{4.1}$$

After dropping the smaller terms, equations (2.6) and (2.7) reduce to

$$\beta\psi_x + \mu J\left[h, h(1-\mu h)\Delta h + \tfrac{1}{2}(1-2\mu h)|\nabla h|^2\right] = 0, \tag{4.2}$$

$$h_t + J(\psi, h) - \beta h(1-\mu h)h_x = 0. \tag{4.3}$$

These are *the governing equations for the thick-upper-layer model.*

Note that in comparison to the thin-upper-layer model (3.2) and (3.3) the nonlinear terms have been dropped in the baroclinic equation (4.3) while the $O(1)$ thickness of the upper layer leads to quartic nonlinearities in (4.2). In the limit as barotropic effects vanish, the model does not reduce to the decoupled model discussed in the previous section but reduces to

$$h_t - \beta h(1-\mu h)h_x = 0. \tag{4.4}$$

This equation has been called the planetary geostrophic wave equation (hereafter PGWE) (Dewar 1987). Given the close relationship between the decoupled model and the thin-upper-layer model, it is of great interest to see if the thick-upper-layer model will exhibit the hyperbolic characteristics of the PGWE. Most notably, the form of the PGWE allows the development of shocks (and shock waves with the appropriate diffusion) given any initial condition (Dewar 1987). (Note that in the limit that the β-effect dominates the nonlinear advection terms, the decoupled model reduces to the PGWE with $\mu = 0$ (see Williams & Yamagata 1984 or Cushman-Roisin 1992) and this results in the long-wave breaking mentioned in § 3.4.)

The PVs for the thick-upper-layer model are given by using the scaling (4.1) in (2.8) and (2.9) giving

$$q_1 = \frac{1}{h} + \sqrt{\varepsilon}\frac{\beta y}{h} + \varepsilon\frac{(1-\mu h)\Delta h - \mu|\nabla h|^2}{h} + O(\varepsilon^{3/2}), \tag{4.5}$$

$$q_2 = \frac{1}{1-\mu h} + \sqrt{\varepsilon}\frac{\beta y}{1-\mu h} - \varepsilon\frac{\mu h\Delta h + \mu|\nabla h|^2}{1-\mu h} + O(\varepsilon^{3/2}). \tag{4.6}$$

4.2. *Linear analysis*

Substitution of (3.7) into (4.2) and (4.3), after some rearrangement, gives

$$\mu h_0'[h_0(1-\mu h_0)(h_0'h' - h_0''h)]' - [\mu h_0(1-\mu h_0)(kh_0')^2 + \beta c + \beta^2 h_0(1-\mu h_0)]h = 0, \tag{4.7}$$

$$h_0'\psi = [c + \beta h_0(1-\mu h_0)]h, \tag{4.8}$$

with the appropriate linear boundary conditions. Once again, the singular point of (4.7) is where the leading-order PV gradients vanish (see (4.5) and (4.6)).

The analyses of Benilov (1992) and Benilov (1995) establish that all fronts are linearly stable. In contrast to the results for the decoupled and thin-upper-layer models, the singular point of the linear equation (4.7) is not a source of linear instability (see Benilov 1995). However, Benilov (1995) also concluded that flows with a vanishing PV gradient can be weakly destabilized by viscosity, ageostrophic or nonlinear effects. Thus, the possibility of an instability is not eliminated within the full nonlinear model, as illustrated in § 5.3.

For the thick-upper-layer model we discuss linear solutions for only a gently sloping front as an exact linear solution for a wedge front does not exist. Given the basic-state flow (3.11) and the conditions that the frontal slope, β-plane effect and frequency are small, (3.12), then to leading order in Δ (4.7) reduces to

$$\tilde{h}'' - \left[k^2 + \frac{\tilde{\beta}}{\mu(1-\mu)\tilde{\alpha}^2}\left(\tilde{c} + \tilde{\beta}(1-\mu)\right)\right]\tilde{h} = 0,$$

with the dispersion relationship

$$\tilde{c} = -\left[\frac{\mu(1-\mu)\tilde{\alpha}^2(k^2+\ell^2)}{\tilde{\beta}} + \tilde{\beta}(1-\mu)\right]. \tag{4.9}$$

The phase velocity and group velocity are always negative and the waves and the energy travel westward regardless of the direction of the basic flow. This is a reflection of the strong influence of the β-plane and the similarity of these waves to westward travelling Rossby waves. If we examine the limit as $\mu \to 0$ we do not get the result of the thin-upper-layer model, but instead get

$$\tilde{c} = -\tilde{\beta},$$

which is the wave velocity of the solution to the decoupled system PGWE as $\mu \to 0$ (see (4.4)).

4.3. *Nonlinear invariants and a stability theorem*

In this subsection we discuss nonlinear invariants of the thick-upper-layer model. It can be established (see Karsten 1998) that

$$\mathscr{E} = \frac{1}{2}\iint_{\mathscr{F}} \mu h\,(1-\mu h)\,|\nabla h|^2 + h(1-\mu h)(\beta y)^2\,\mathrm{d}x\,\mathrm{d}y, \tag{4.10}$$

$$\mathfrak{C}_1 = \iint_{\mathscr{F}} \Phi_1(h)\,\mathrm{d}x\,\mathrm{d}y, \tag{4.11}$$

$$\mathfrak{C}_2 = \iint_{\mathscr{F}} y\Phi_2(h)\,\mathrm{d}x\,\mathrm{d}y, \tag{4.12}$$

are invariant for equations (4.2) and (4.3). $\mathscr{E}$ is the pseudo-energy invariant and $\mathfrak{C}_{1,2}$ are PV invariants (the first is the leading-order PV invariant in both layers and the second a combination of the higher-order PVs). Note that the zonal momentum impulse associated with the upper layer given by (3.22) is special case of (4.12) and therefore an invariant of the flow.

The nonlinear stability argument presented for the thin-upper-layer model follows accordingly for the thick-upper-layer model. The only change is the differing form of $\mathfrak{C}_2$. This leads to the following theorem:

THEOREM 4.1. *The zonal flow $h_0(y)$ is nonlinearly stable in the sense of Liapunov*

with respect to the perturbation norm (3.23) if there exist real constants A and B such that either

$$0 < A < \Phi_1''(\xi) + y\Phi_2''(\xi) < B < \infty, \ \forall \ \xi \geqslant 0 \quad \text{and} \quad y \in [W_1, W_2], \tag{4.13}$$

or

$$-\infty < A < \Phi_1''(\xi) + y\Phi_2''(\xi) < B < 0, \ \forall \ \xi \geqslant 0 \quad \text{and} \quad y \in [W_1, W_2], \tag{4.14}$$

where

$$\Phi_1'(h_0) + y\Phi_2'(h_0) = 0. \tag{4.15}$$

As in § 2.3, one can also establish linear stability if (4.15) holds and $\delta^2\mathfrak{I}(h_0)$ is definite and conserved by the linear equations. If (4.13) or (4.14) holds for all $\xi = h_0(y)$, then $\delta^2\mathfrak{I}(h_0)$ is definite. Once again, an extra condition is required in order to establish that $\delta^2\mathfrak{I}(h_0)$ is conserved, namely that

$$\frac{\mathrm{d}^2}{\mathrm{d}y^2}\Phi_2(h_0) = 0, \ \forall \ y \in [W_1, W_2]. \tag{4.16}$$

Conditions (4.15) and (4.16) imply that

$$\Phi_1''(h_0) + y\Phi_2''(h_0) = \frac{C}{(h_0')^2}$$

for some arbitrary constant C. Thus, (4.13) or (4.14) can hold for all $\xi = h_0(y)$ only if $h_0' \neq 0 \ \forall \ y \in [W_1, W_2]$. Thus, one obtains a weaker stability result than that of Benilov (1992): all strictly monotonic fronts are stable but we cannot establish the stability if $h_0' = 0$.

In order to interpret the nonlinear stability result we proceed as in § 3.3, and choose the PV invariants so that $\mathfrak{I}$ is the momentum invariant constrained by the first PV invariant (4.11) giving (3.28). The analysis in § 3.3 follows giving that all smooth, strictly non-monotonic fronts are nonlinearly stable. If we try to proceed as in § 3.3 and repeat the procedure using the second PV invariant (4.12) we run into difficulty since the momentum invariant is a special case of (4.12). If we choose $\mathfrak{I}$ to be the momentum invariant constrained by the second PV invariant, as in (3.30), then (4.15) requires $\Phi_2'(h_0) = 1$, and, thus, $\Phi_2''(h_0) = 0$. As such, neither condition (4.13) or (4.14) can be met. All other attempts at constructing a suitable nonlinear invariant have resulted in the same result: if $h_0' = 0$ stability cannot be established. As in the decoupled model, the singular point is a possible source of nonlinear instability (see § 5.3).

4.4. *Finite-amplitude analysis*

In this subsection, the effects of nonlinear terms in the model are examined for the gently sloping front as in § 3.4. Repeating the analysis of a slowly varying wave-train once again leads to the amplitude equation (3.32) and we have the stability parameter

$$\Gamma_1 = -\frac{2k^2\ell^2(k^2 - 9\ell^2)}{9\alpha^2(k^2 - \ell^2)}$$

(see Karsten 1998 for details). Thus, the regions of stability/instability are easily defined. For $\ell < k < 3\ell$, $\Gamma_1 < 0$ and the wave-train is stable. For $k < \ell$ or $k > 3\ell$, $\Gamma_1 > 0$ and the wave-train is subject to BF instability.

Again, the LWSW resonance, which occurs when $k = \ell$, is important. If we carry

out the analysis found in § 3.4 for the thick-upper-layer model we once again obtain (3.38) and (3.39) with

$$\Gamma_2 = 8k^3\ell^2\mu^2(1-\mu)^2(3\ell^2 - k^2).$$

Once again the Stokes wave solution is subject to instability.

Thus, at large zonal scales, the LWSW resonance leads to unstable growth. At zonal scales slightly smaller than meridional scales, there is a small region of stability. At small zonal wavelengths the growth rate of the BF instability becomes comparable to and eventually exceeds the growth rate associated with the LWSW resonance. These results are similar to those for the thin-upper-layer model with small differences. Most notably, the results are symmetrical for eastward and westward flows. Note that this is predicted by the thin-upper-layer model in the limit as $\mu \to \infty$ (see the discussion in § 3.4). Though the non-dimensional growth rates are smaller for the thick-upper-layer model, dimensional growth rates are actually somewhat larger. We expect a greater increase in the growth rate as the amplitude of the flow increases.

5. Numerical simulations

In this section, the strong-β models are solved using a straightforward numerical scheme. We concentrate on the instabilities associated with the PV singularities. It is these instabilities that will produce large-amplitude waves that will best reflect the finite-amplitude results of § 3 and § 4.

It should be noted that all the LAG models handle outcroppings with ease, with no additional code to specify the location of the outcropping. This advantage results from the fact the baroclinic equation is given in terms of the upper-layer depth h and is trivially satisfied when $h = 0$ and, importantly, the appropriate *dynamic* boundary condition on an outcropping is the upper-layer PV equation itself when evaluated on the outcropping (Swaters 1993*b* and Karsten 1998). Thus, as long as the frontal height is continuous across an outcropping, the baroclinic equation applies equally well on either side of the outcropping.

The algorithm we use is straightforward: an explicit, finite-difference scheme that is leapfrog in time and central in space. The Jacobian terms are approximated using the Arakawa (1966) scheme. The simulations are run in a zonally periodic channel with no-normal-flow conditions at the channel walls. The geometry of the flow is chosen to limit the effect the channel walls have on its evolution. For the baroclinic equation, the algorithm is similar to that used in Reszka & Swaters (1999) and Swaters (1998).

However, the barotropic equation found in the strong-β model is diagnostic and is simply integrated at each time step. This only determines the barotropic stream function ψ up to an arbitrary function independent of x. That is, the barotropic equation allows for an arbitrary, evolving zonal flow. Determining this arbitrary flow is not a trivial matter as we have no equation for the time evolution of the mean barotropic flow. Rearranging the full equations to solve for this arbitrary flow leads to an equation that is numerically infeasible. Our approach is to simply impose that the zonal flow maintain its initial value, generally taken to be zero. It should be noted that this will allow the code to capture linear wave behaviour which does not result in changes to the mean flow, but does not allow the nonlinear interactions of waves to produce a zonal barotropic response.

We employ two types of numerical friction. The first eliminates negative values of the frontal height. These values are not physical, since the frontal height is necessarily a non-negative quantity, and are simply set to zero. In effect, this is a delta-function

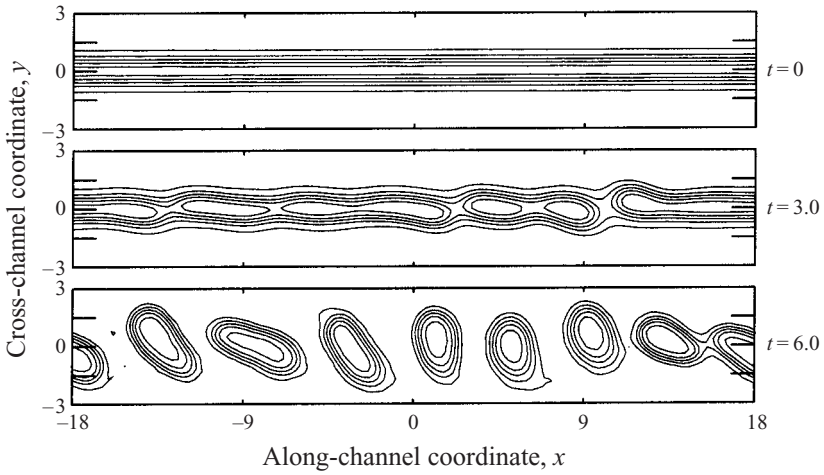

FIGURE 4. Results of the numerical simulation of the decoupled model for the coupled front simulation. The graphs show the contours of the upper-layer height with a contour interval 0.1.

friction acting on the scale of the numerical grid itself. Secondly, we make use of high-power harmonic friction to smooth results by eliminating small-scale waves. We chose to use Δ^8 friction. Note that a high-power harmonic friction is necessary to overcome the cubic and quartic nonlinearities and the fourth-order derivatives found in model equations. Use of numerical friction does affect the conservation of the model invariants by dissipating energy at small scales.

5.1. *Decoupled model*

We present the decoupled model simulations first as they share many characteristics with the thin-upper-layer model but are less expensive to run and allow a clear demonstration of slow nonlinear effects. Simulations were run to examine the implications of the finite-amplitude analysis. In these simulations, there was a slow cascade of energy to large scales, even when no friction was used. Simulations did not developed large-scale structures that could be clearly identified as wave packets or solitons. However, perturbations were often reorganized into zonal jets. In fact, for gently-sloping fronts, the LWSW resonance dominated all such simulations resulting in a final-state perturbation field consisting of alternating zonal jets across the domain. Such a final state is predicted in the work of Rhines (1975). With a large-amplitude front, the jets tend to be restricted to regions where the flow is strongest.

As well, simulations have been computed for fronts where a vanishing PV gradient allows for linear instability (Benilov 1995). For these simulations, the frontal profile is a simple Gaussian corresponding to two jets of equal strength but opposite in direction. In Griffiths *et al.* (1982), such fronts are examined and also an instability which arises from the coupling of the free streamlines and, hence, these fronts are referred to as coupled fronts. These simulations lead to the breakup of a strongly sheared current into a series of propagating eddies (see Karsten 1998). Our decoupled model simulations extend the calculations of Pavia (1992) to include a β-plane which results in a westward drift of the eddies (see Karsten 1998 and Chassignet & Cushman-Roisin 1991 for further discussion of eddy drift). For comparison to the two-layer models we present the structure of the evolution of the front in figure 4. As

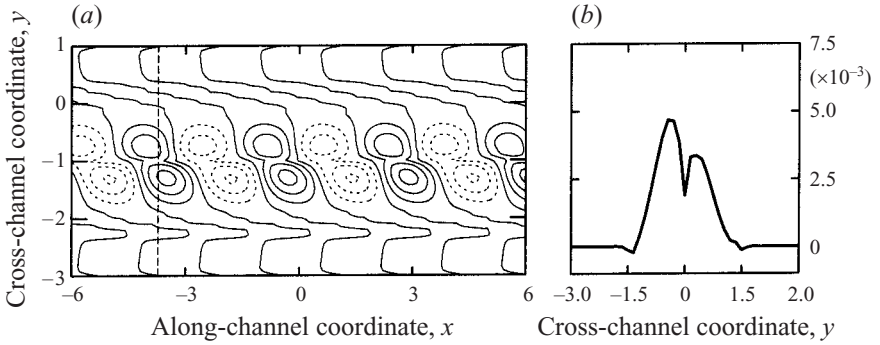

FIGURE 5. The structure of the growing wave: (*a*) the contours of a growing wave (dashed contours are negative values); (*b*) the cross-section through the wave indicated by the dashed line on the contour plot.

the instability grows, the front develops large meanders and eventually forms into a series of westward propagating, rotating ovular eddies.

In figure 5 the structure of a growing wave is plotted. This wave is taken from a simulation initialized with a single frequency known to be unstable. The perturbation consists of two waves, each associated with one of the jets of the coupled front, with the northern (upper) wave shifted westward from the southern (lower) wave. The profile of the wave shows that the waves overlap each other resulting in a cusp which lies directly over the singular point where the frontal PV gradient vanishes. The growth of the instability is dependent on the interaction of the two waves. If the front is too wide, each current supports stable travelling waves. It should be noted that as the instability grows, it shifts to larger scales (see the discussion in § 5.2).

In general, the instabilities associated with the vanishing PV gradient illustrate the characteristic described in Benilov (1995). The instability has a high- and low-wavenumber cutoff. Increasing β reduces the growth rate while shifting the instability to smaller scales. On the other hand, increasing the maximum slope increased the growth rate. We also note that the instability existed for fronts associated with both an increase in the upper-layer depth and a decrease, producing anticyclonic and cyclonic eddies respectively. The growth rate for anticyclonic eddies is much greater than for cyclonic eddies as the greater depth of fluid where the singularity occurs results in a greater growth rate. Thus, the LAG model *favours the growth of anticyclonic eddies* within a thin frontal layer. Finally, outcroppings appear to have little effect on the growth of instabilities. It is not essential that there be a coupling of 'free streamlines', only a coupling of the waves supported by each jet. The fact that such instabilities exists in the decoupled model stresses their barotropic nature. Indeed, the instability results from a release of kinetic energy from the mean flow but little release in mean potential energy (PE).

The idealized coupled fronts are not generally common in the oceanic observations, possibly due to their highly unstable nature. However, it is not uncommon for surface forcing to produce regions of counterflow within a large-scale current (see Roden 1975 and Benilov & Reznik 1996). These flows should produce an instability, resulting in large-amplitude waves on the front, which then should proceed to form large-scale structures. Thus, changing structures of the front can result in a source of instability eventually leading to large-scale meanders of a front. Thus, the final simulation for

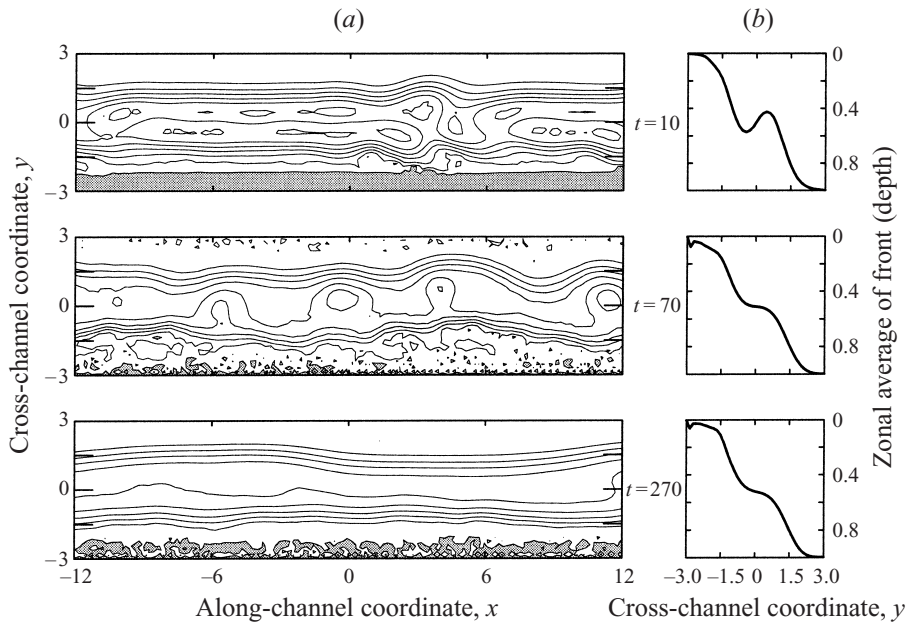

FIGURE 6. Results of the numerical simulation of the decoupled model for an isolated front with shear. (*a*) The contours of the upper-layer height. The grey regions are regions where the upper layer vanishes and the contour interval is 0.1. (*b*) The zonally averaged upper-layer height versus y.

the strong-β models is run on an isolated front with a sheared flow that has a small jet of return flow (see figure 6, $t = 0$ for a cross-section of the front).

The results of this simulation are shown in figure 6 which plots contours of frontal height and cross-sections of zonally averaged height. The shear in the flow allows unstable growth at the scales associated with the counterflow ($k = 2$). After the instability has grown, and the frontal shear has been eliminated, we see the cascade of energy to larger scales resulting in a front with a persistent large-zonal-length scale, small-amplitude meander.

It should be noted that the drop in kinetic energy associated with the elimination of the counter-jet is balanced by a movement of frontal fluid southward (see figure 6) as required by the conservation of $\mathscr{E}$. Alternatively, the fact that this flow of fluid south can occur allows a release of baroclinic kinetic energy (KE), feeding the growth of the instability and the development of the waves. The simulation clearly indicates that meanders can develop and be maintained as a result of a sheared flow with little release of PE.

5.2. *Thin-upper-layer model*

For the thin-upper-layer model, we wish to examine how the addition of a coupled barotropic flow affects the evolution of the fronts discussed above. As with the decoupled model, stable fronts do allow the reorganization of waves into larger structures and zonal jets as discussed in § 3.4. Small-scale waves were dissipated more rapidly and the asymmetry between eastward and westward flows was more acute in the thin-upper-layer limit.

Instead of giving quantitative detail for stable flows, we focus on the instabilities associated with the vanishing PV gradients. In terms of these instabilities, we have conflicting theoretical results: linear instability (Benilov 1995) but nonlinear stability

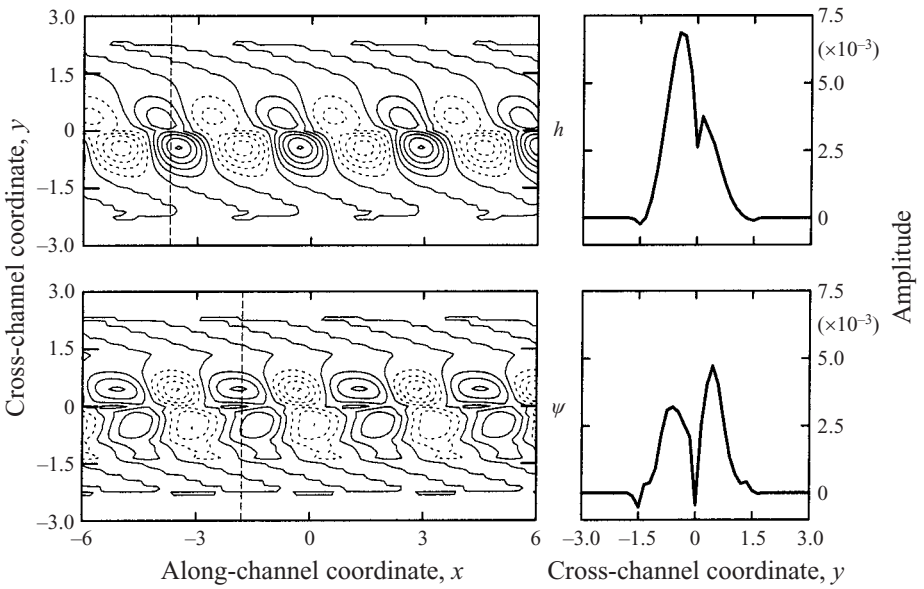

FIGURE 7. The structure of the growing wave. The upper plots are for the perturbation frontal height, the lower plots for the barotropic stream function. (*a*) The contours of a growing wave (dashed contours are negative values). (*b*) The cross-section through the wave indicated by the dashed line on the contour plots.

(§ 3.3). However, in the numerical simulations we expect the linear results to manifest themselves for two reasons. First, numerical simulations which include friction do not exactly conserve the invariants which the theory in § 3.4 depend on. Second, imposing a vanishing mean barotropic flow imposes a restriction on the nonlinear evolution but not the linear evolution.

For the singularity $h_0' = 0$, the addition of the weak lower-layer dynamics has little effect on the results and, contrary to the analysis of § 3.3, a vigorous instability develops. Simply put, the evolution of the front is dominated by the baroclinic equation. In figure 7 we plot the growing perturbation of a typical coupled front simulation for the thin-upper-layer model. The structure of the frontal depth perturbations is similar to the decoupled case (see figure 5) but shows a markedly stronger asymmetry between the two jets. The associated barotropic stream function cells are opposite in sign, stronger on the northern jet as opposed to southern and shifted eastward by one quarter of a wavelength. A sharp cusp at the PV singularity ($y = 0$) is notable in both the baroclinic and barotropic modes.

In figure 8, we examine the tendency of the instability to progress to larger scales as the amplitude increases. For comparison, we have included the analogous decoupled result as a dashed line. We plot the amplitude versus wavenumber at four different times. Initially, the wave grows quickest at approximately $k = 2.3$ but as the time proceeds and the wave reaches larger amplitude the maximum growth shifts to smaller values of k and hence large scales. That is, initially shorter waves grow faster but then their amplitude is modulated. Longer waves grow continually reaching a much larger amplitude and finally producing the eddies. This cascade to larger scales by an unstable wave is discussed in greater detail in Part 2, where a finite-amplitude analysis illustrates that weak-β models can experience nonlinear modulation of waves at small scales but nonlinear growth at large scales. In agreement with Benilov (1995), growth

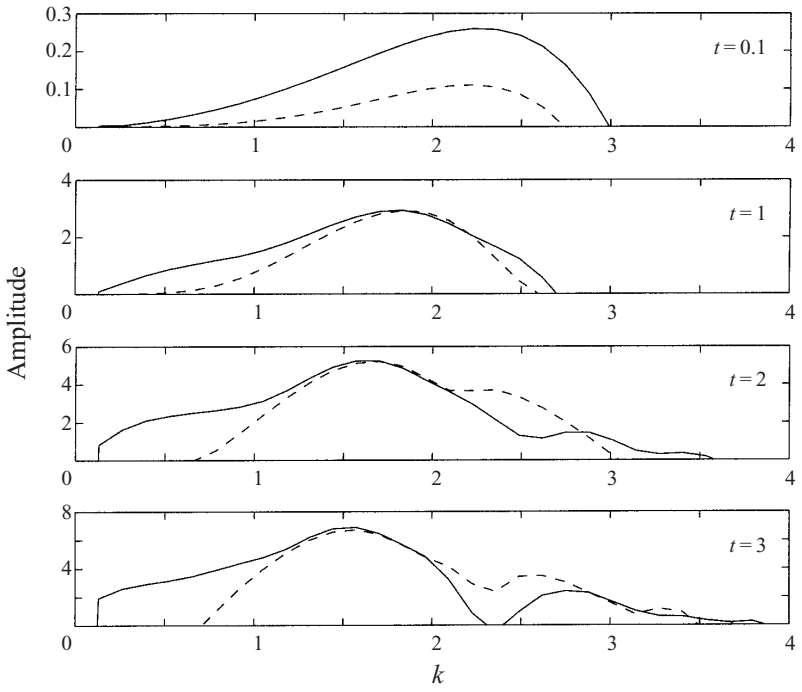

FIGURE 8. Plots of the amplitude of the waves versus wavenumber as the front evolves. The dashed lines are the corresponding values for the decoupled model.

occurs at the largest scales for the thin upper layer while the decoupled model has a low-wavenumber cutoff for instability. Initially, the instability in the thin-upper-layer model grows much faster as the coupling to the barotropic flow means the unstable modes are excited sooner.

As the instability progresses we see the breakup of the front into a series of eddies, almost identical to that shown in figure 4. Coupled to these eddies are weak barotropic cells which reduce the westward propagation of the eddies. And when such an instability is included within a large front, the addition of the lower layer increases the rate at which energy cascades to larger scales, once again resulting in large waves propagating along the front.

Fronts that include the singular point $h_0' = -\beta$ are also linearly unstable, though the growth rates associated with the linear instability are small, roughly an order smaller than those associated with the singular point $h_0' = 0$ (see Benilov 1995). Such instabilities were found in our simulations, though they require significant time to develop. We examine such an instability in figures 9 and 10. In figure 9 we illustrate the initial form of a front and the final state after finite-amplitude waves have grown. In figure 10, we plot the form of the growing perturbation. The front is quadratic in form with a lower-layer PV singularity at $y = 0.94$. The perturbation forms as a baroclinic monopole with some structure at the outcropping and an associated dipole in the barotropic flow. The maximum amplitude of the wave is shifted northward from the PV singularity and the wave is smooth across the singularity (compare this to figure 8). The perturbation grows slowly (an e-folding time of 80 days) to finite size producing a large frontal wave (wavelength 1000 km) whose amplitude then oscillates in time. This weak instability may be dominated by the stabilizing effects

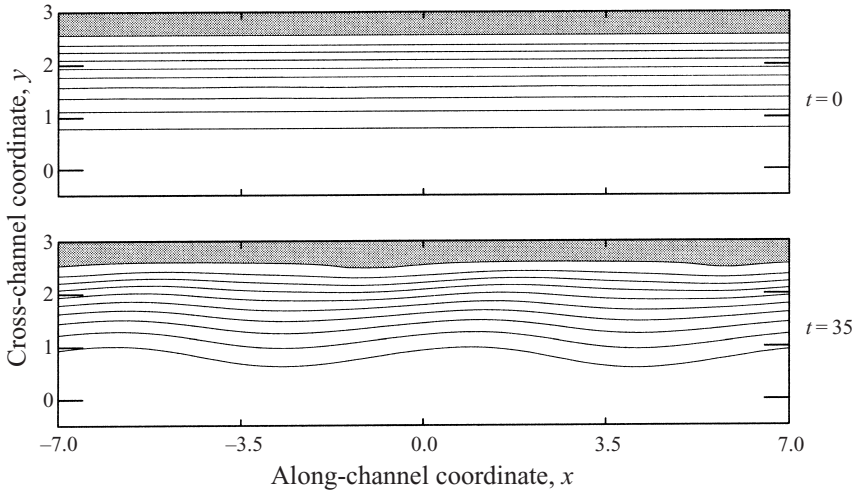

FIGURE 9. Contour plots of the front initially and after the instability has grown into a large wave. The grey regions are regions where the upper layer vanishes and the contour interval is 0.1.

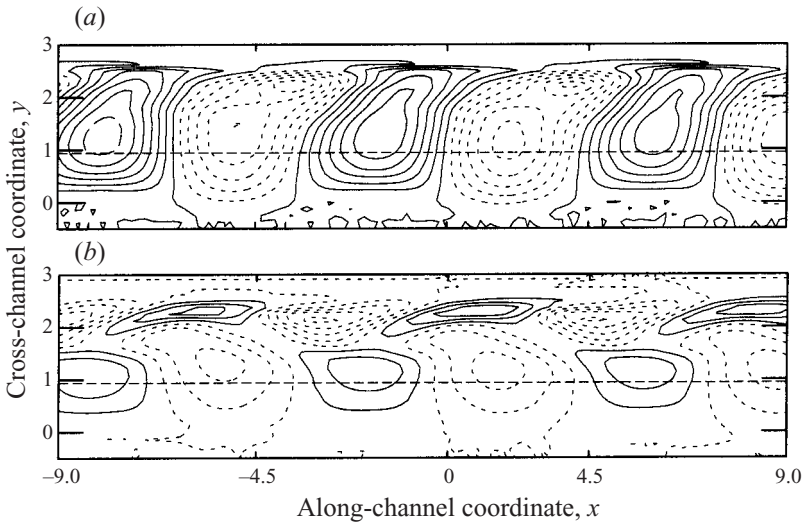

FIGURE 10. Contour plots of the growing wave: (*a*) the perturbation frontal depth, (*b*) the barotropic stream function. Dashed contours are negative. The dashed horizontal line marks the location of the lower-layer PV singularity.

of the nonlinear terms and friction or the vigorous instability associated with the upper-layer PV singularity.

5.3. *Thick-upper-layer model*

The analysis of §4 suggests that with the thick-upper-layer model stable waves will also reorganize into larger wave packets and possibly develop zonal jets. As with a thinner upper layer, numerical simulations support these results. Eastward and westward flows are now symmetric and the cascade of energy to larger scales is non-dimensionally slower as the theory predicted.

More interesting simulations are those for a coupled front where the PV gradient

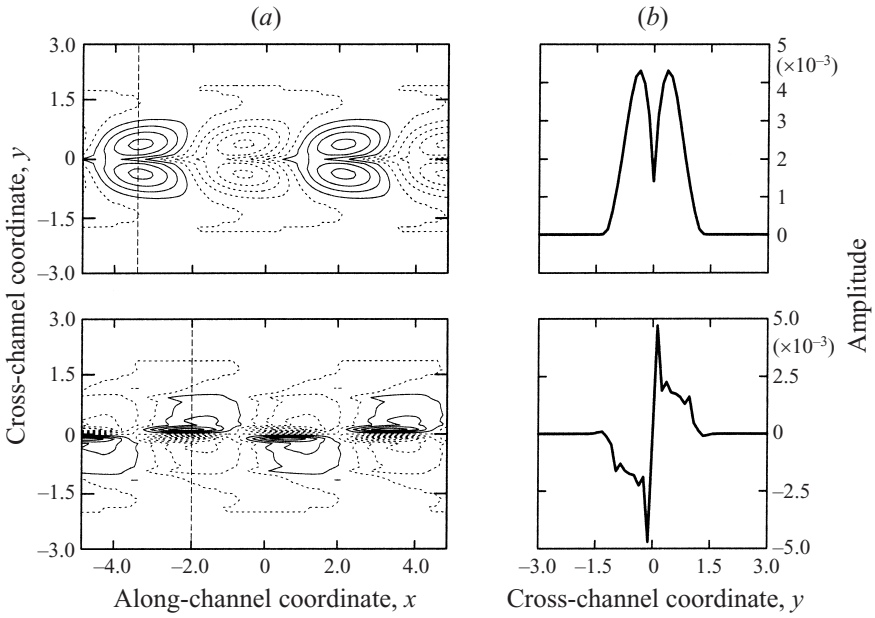

FIGURE 11. The structure of the growing wave. The upper plots are for the perturbation frontal height, the lower plots for the barotropic stream function. (*a*) Shows the contours of a growing wave (dashed contours are negative values); (*b*) the cross-section through the wave indicated by the dashed line on the contour plot.

vanishes. Surprisingly, a barotropic instability does grow. This appears to contradict the results of Benilov (1995) which indicated that the singular point $h_0' = 0$ is not a source of instability. However, Benilov (1995) also concluded that the stability is 'structurally unstable' and that it is possible that such fronts 'can be weakly destabilized by small viscosity ageostrophic effects or external forcing'. Thus, the instability could be a result of friction or a nonlinear effect. To attempt to answer this question we plot the form of a growing wave at small amplitudes.

In figure 11, we plot the structure of the perturbation that grows. The perturbation is a symmetric structure about the point where the PV gradient vanishes ($y = 0$) but has a sharp cusp across this point. This is manifested as small-scale dipole in the barotropic stream function, with a sharp gradient at $y = 0$. Such a sharp jump involves large gradients and, thus, the nonlinear frontal terms are large in amplitude. As well, the large gradients result in a large amount of friction allowing such a jump to be smoothed on small scales. Therefore, both factors enter into this instability. The growth rate of these waves increases with the strength of the shear in the flow and decreases with β. For typical values, $R_I = 35\,\text{km}$, and $\epsilon = 0.1$, the fastest growing waves have an e-folding time of 12 days and a wavelength of 770 km, roughly 3.5 times the width of the front.

As this instability grows, the waves grow to large amplitude. As they reach finite amplitude they break, as they are dominated by the hyperbolic nature of the baroclinic equation. In figure 12, we plot the contours and an along-front section of the front which clearly illustrates the breaking waves. In some simulations, the effects of friction were able to balance the wave breaking, resulting in travelling shock waves that took the form of tear-drop-shaped eddies. If a coupled front is excited by numerous scales,

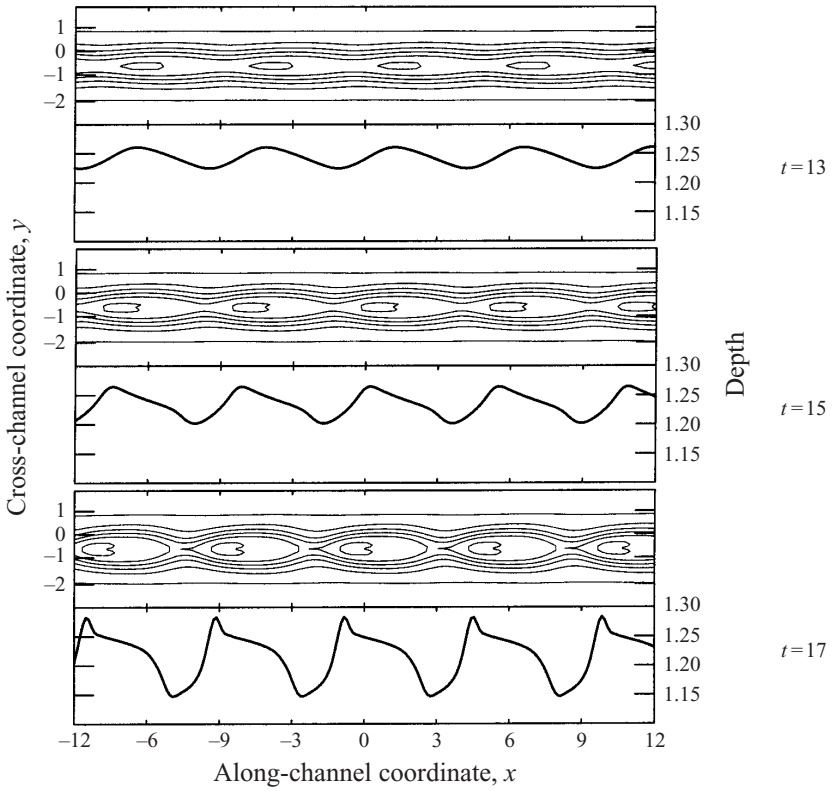

FIGURE 12. An example of a wave as it breaks. For three times we plot contours of the upper-layer depth (upper plot) and a cross-section through $y = 0$ (lower plot).

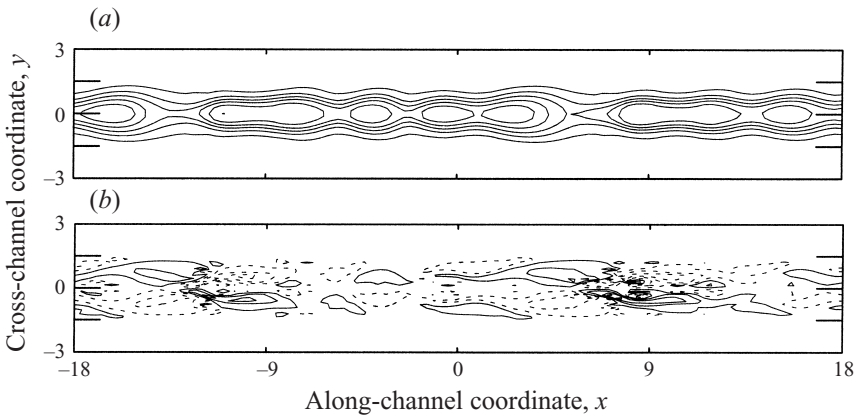

FIGURE 13. Results of the numerical simulation of the thick-upper-layer model coupled front simulation: (*a*) the contours of the upper-layer height, (*b*) the contours of the barotropic stream function. Dashed contours indicate negative values.

this can result in a series of westward propagating 'eddies' with associated barotropic dipoles as illustrated in figure 13.

It should be noted that this instability is crucially dependent on the coupling of the baroclinic and barotropic flows. When decoupled, the dynamics are governed by the

β-effect	Layer depths	Baroclinic	Barotropic	Analysed in
Strong	Thin upper	LAG_β	β-LAG	Part 1
Strong	Thick upper	CPG_β	β-LAG	Part 1
Weak	Equal layers	CPG	QG_β-LAG	Part 2
Weak	Thin upper	LAG	QG_β-LAG	Part 2

TABLE 1. Classification of barotropic and baroclinic equations. Abbreviations are defined in the text.

PGWE which has travelling-wave solutions, which eventually break to form shocks (see Dewar 1987). Thus, it appears that in the two-layer dynamics it is the coupling of the barotropic and baroclinic modes that allows the unstable small perturbations. Once these perturbations have grown to finite size, the resulting wave is governed by the PGWE equation and eventually breaks.

Once again, the inclusion of a PV singularity in a large front can lead to long waves. This instability develops slower than for the thin-upper-layer model (in non-dimensional units) and persists for some time. The long waves are not as robust as those seen in the thin-upper-layer model, as they are subject to wave breaking. Once again there is a movement of fluid as the shear flow is removed. The front flattens as $h(1-\mu h)y^2$ increases, allowing a release of baroclinic KE as in the thin-upper-layer model.

6. Conclusions

Before summarizing the results of this paper, we briefly compare the structure of the LAG models studied here as well as the weak-β models examined in Part 2. In table 1, we include a description of the baroclinic and barotropic equations using the terms QG, CPG (coupled planetary geostrophic; see de Verdiére 1986), LAG and β. We used these terms based on the similarity of the equations to previously derived models that use similar nomenclature. As such, QG is applied to models that involve the evolution of relative vorticity terms, CPG is applied to models that are dominated by layer depth changes and the coupling of the two layers, and LAG is applied to models that include the nonlinear advection terms associated with large-amplitude frontal effects. The label β is used in two manners. When written in regular type it signifies a model that is dominated by the background vorticity gradient provided by the β-plane effect. When used as a subscript, it indicates that the model includes β-plane effects.

The baroclinic equation can be described as one of the first three types of models. The barotropic equation, representing a balance between baroclinic and barotropic effects, is a balance between two forms of equations. In columns three and four of table 1 we list the appropriate description of each equation for the given model. In the description of the barotropic equation we list the barotropic component first and then the baroclinic component.

From table 1, the effect of altering the β-plane effect and the layer depths is clear. As the strength of the β-plane effect increases, it eventually dominates the relative vorticity terms of the barotropic flow giving rise to the strong-β models where the barotropic equation is β-LAG in form. If the β-plane effect is weak, the relative vorticity terms enter the leading-order barotropic equation which is now QG-LAG in form. As the depth ratio increases, the coupling between the two layers becomes

more important and dominates the frontal effects. Thus, the baroclinic equation for the models where the layers are scaled equally are CPG in form while the models where the upper layer is thinner are LAG in form. When the β-plane effect is strong, it enters into the baroclinic equation and hence the leading-order dynamics. As such, these models are more closely related to PG dynamics rather than QG dynamics.

The classification above can also lead to insight into the stability of fronts described by a given model. In general, the background vorticity gradient of the β-plane is a stabilizing force while QG effects are destabilizing forces. For the strong-β models, we expect fronts to be baroclinically stable since the β-plane dominates the source of baroclinic instability, the QG effects. Frontal effects tend to steepen the front, favouring the formation of robust, large-scale structures (see Cushman-Roisin & Tang 1992 and Tang & Cushman-Roisin 1992). Thus, we expect a cascade of energy to larger scales. Frontal effects also allow barotropic instability. However, strong coupling dominates the frontal effects in the leading-order dynamics and it is expected that the hyperbolic nature of the β-plane effect will produce breaking waves.

These expected results are indeed what we find in the nonlinear examination of this paper. For all strong-β models, fronts are linearly and nonlinearly stable unless the PV gradients vanish. The finite-amplitude analysis suggests that stable waves should reorganize themselves into wave packet/soliton structures or possibly zonal jets via BF instability and LWSW resonances. Numerical simulations illustrate that large-scale structures and/or zonal jets do develop but they are small in amplitude.

All strong-β models allow for unstable growth associated with vanishing PV gradients. For a thin front, the PV singularities provide two sources for large frontal waves. The upper-layer PV singularity gives rise to a vigorous instability resulting in eddies with scales on the order of the flow's width. Within a larger front, these eddies are reorganized via the nonlinear cascade discussed above into large frontal waves. The effect of the lower layer on this instability is small. Unlike QG models, the LAG model favours the growth of anticyclonic eddies within a thin frontal layer in accordance with primitive equations and observations (Boss, Paldor & Thompson 1996). The lower-layer PV singularity also results in an instability, but one with a very slow growth rate which produces large frontal waves directly. When the coupling is very strong, the PV singularities coincide and eastward and westward flows give identical results. An instability still grows, but it is dependent on the nonlinear coupling of the two layers. The large-amplitude waves which result are governed by the hyperbolic nature of the baroclinic equation and eventually break.

Finally, while outcroppings can be easily included in the LAG models, they were found to have little effect on the dynamics of the strong-β models. At the length scales of the strong-β model, the details associated with outcropping dynamics are not properly resolved.

In conclusion, as the β-plane effect becomes strong and begins to dominate QG effects we see a transition to the Rossby wave regime discussed in Tang & Cushman-Roisin (1992). In this regime, there is 'little vertical energy transfer' and the flow 'amounts to no more than the dispersion of Rossby waves' (Tang & Cushman-Roisin 1992). However, the possibility of barotropic instability can provide a source for the production of these Rossby waves, and thus, the release of mean kinetic energy.

An obvious extension of this work is the examination of several-layer models (see Benilov & Sakov 1997). The addition of more layers allows the examination of more complicated physical processes and the modelling of more realistic situations (see Spall 1995). However, one cannot simply match any models together as the middle layer must describe dynamics at equivalent scales for both models. And it is not

obvious whether multi-layered models would result in instabilities not seen in the two-layer models. How three-, or possibly four-layer LAG models can be used to accurately describe systems with both surface and bottom currents requires further investigation.

Another aspect of the analysis we have not focused on is the variation of Rossby wave speed as we move from QG dynamics to LAG dynamics, and from linear to fully nonlinear amplitudes. Recent observations of Rossby waves (Chelton & Schlax 1996) have indicated that baroclinic Rossby waves propagate faster than predicted by standard QG theory, suggesting a more important role of the mean flow, nonlinear interactions and/or topography. The strong-β models offer an excellent framework to examine some of these questions.

As well, a study of how two-layer LAG models could be used to improve ocean general circulation models could be undertaken. As mentioned in the introduction, stable fronts play a role in the subduction of equatorward flow. Modelling such subduction is an active area of research (see Spall 1995). The LAG models studied here allow a simple two-layer model of generally stable fronts to be studied both analytically and numerically. The addition of wind stress and buoyancy forcing to the models would allow more realistic situations to be examined. Such forcing could create and sustain the type of sheared flow examined here, thus providing a continual source of instability. As well, the LAG models allow measurements of the inertial terms associated with the frontal effects not present in analysis based on a QG assumption. Further work continues in these areas, and the results will doubtlessly prove very interesting.

Our thanks to Eugene Benilov and an anonymous referee whose suggestions greatly improved the final text. Preparation of this paper was supported in part by Natural Sciences and Engineering Research Council of Canada (NSERC) Research Grants awarded to G. E. S. and a NSERC Postgraduate Scholarship, Killam Doctoral Fellowship and NSERC Postdoctoral Fellowship awarded to R. H. K.

REFERENCES

Anderson, D. L. T. & Killworth, P. D. 1979 Nonlinear propagation of long Rossby waves. *Deep-Sea Res.* **26A**, 1033–1050.

Arakawa, A. 1966 Computational design for long term numerical integration of the equations of fluid motion: two-dimensional incompressible flow. *J. Comput. Phys.* **1**, 119–143.

Barth, J. A. 1989 Stability of a coastal upwelling front. 1. Model development and a stability theorem. *J. Geophys. Res.* **94**, 10844–10856.

Benilov, E. S. 1992 Large-amplitude geostrophic dynamics: the two layer model. *Geophys. Astrophys. Fluid Dyn.* **66**, 67–79.

Benilov, E. S. 1993 Baroclinic instability of large-amplitude geostrophic flows. *J. Fluid Mech.* **251**, 501–514.

Benilov, E. S. 1994 Dynamics of large-amplitude geostrophic flows: the case of 'strong' beta-effect. *J. Fluid Mech.* **262**, 157–169.

Benilov, E. S. 1995 On the stability of large-amplitude geostrophic flows: the case of 'strong' beta effect. *J. Fluid Mech.* **284**, 137–158.

Benilov, E. S. & Cushman-Roisin, B. 1994 On the stability of two-layered large-amplitude geostrophic flows with thin upper layer. *Geophys. Astrophys. Fluid Dyn.* **76**, 29–41.

Benilov, E. S. & Reznik, G. M. 1996 The complete classification of large-amplitude geostrophic flows in a two layer fluid. *Geophys. Astrophys. Fluid Dyn.* **82**, 1–22.

Benilov, E. S. & Sakov, P. V. 1997 Dynamics of large-amplitude flows over bottom topography. *Nonlinear Process. Geophys.* **4**, 55–62.

Boss, E., Paldor, N. & Thompson, L. 1996 Stability of a potential vorticity front from quasi-geostrophy to shallow water. *J. Fluid Mech.* **315**, 65–84.

Charney, J. G. & Flierl, G. R. 1981 Oceanic analogues of large-scale atmospheric motions In *Evolutions of Physical Oceanography* (ed. B. A. Warren & C. Wunsch), pp. 504–548. The MIT Press.

Chassignet, E. P. & Cushman-Roisin, B. 1991 On the influence of a lower layer on the propagation of nonlinear oceanic eddies. *J. Phys. Oceanogr.* **21**, 939–957.

Chelton, D. B. & Schlax, M. G. 1996 Global observations of oceanic Rossby waves. *Science* **272**, 234–238.

Craik, A. D. D. 1985 *Wave Interactions in Fluid Flows*. Cambridge University Press.

Cushman-Roisin, B. 1986 Frontal geostrophic dynamics. *J. Phys. Oceanogr.* **16**, 132–143.

Cushman-Roisin, B., Sutyrin, G. G. & Tang, B. 1992 Two-layer geostrophic dynamics. Part I: Governing equations. *J. Phys. Oceanogr.* **22**, 117–127.

Cushman-Roisin, B. & Tang, B. 1990 Geostrophic turbulence and the emergence of eddies beyond the radius of deformation. *J. Phys. Oceanogr.* **20**, 97–113.

Dewar, W. K. 1987 Planetary shock waves. *J. Phys. Oceanogr.* **17**, 470–482.

Djordjevic, V. D. & Redekopp, L. G. 1977 On two-dimensional packets of capillary-gravity waves. *J. Fluid Mech.* **79**, 703–714.

Flierl, G. R., Malanotte-Rizzoli, P. & Zabusky, N. J. 1987 Nonlinear waves and coherent vortex structures in barotropic β-plane jets. *J. Phys. Oceanogr.* **17**, 1408–1438.

Griffiths, R. W., Killworth, P. D. & Stern, M. E. 1982 Ageostrophic instability of ocean currents. *J. Fluid Mech.* **117**, 343–377.

Griffiths, R. W. & Linden, P. F. 1981 The stability of buoyancy-driven coastal currents. *Dyn. Atmos. Oceans* **5**, 281–306.

Griffiths, R. W. & Linden, P. F. 1982 Laboratory experiments on fronts. Part 1: Density-driven boundary currents. *Geophys. Astrophys. Fluid Dyn.* **19**, 159–187.

Grimshaw, R. H. J. 1977 The modulation of an internal gravity-wave packet, and the resonance with the mean motion. *Stud. Appl. Maths* **56**, 241–266.

Ikeda, M. & Emery, W. J. 1984 Satellite observations and modelling of meanders in the California current system off Oregon and Northern California. *J. Phys. Oceanogr.* **14**, 1434–1450.

Ikeda, M., Emery, W. J. & Mysak, L. A. 1984 Seasonal variability in meanders of the California current system off Vancouver Island. *J. Geophys. Res.* **89**, 3487–3505.

Karsten, R. H. 1998 Nonlinear effects in two-layer, frontal-geostrophic models of surface ocean fronts. PhD thesis, Department of Mathematical Sciences, University of Alberta.

Karsten, R. H. & Swaters, G. E. 1996 A note on the stability theory of buoyancy-driven ocean currents over a sloping bottom. *Z. Angew Math. Phys.* **47**, 28–38.

Karsten, R. H. & Swaters, G. E. 1999 A unified asymptotic derivation of two-layer, frontal geostrophic models including planetary sphericity and variable topography. *Phys. Fluids* **11**, 2583–2597.

Karsten, R. H. & Swaters, G. E. 2000 Nonlinear effects in two-layer large-amplitude geostrophic dynamics. Part 2. The weak-beta case. *J. Fluid Mech.* **412**, 161–196.

Killworth, P. D. 1983 Long wave instability of an isolated front. *Geophys. Astrophys. Fluid Dyn.* **25**, 235–258.

Killworth, P. D., Paldor, N. & Stern, M. E. 1984 Wave propagation and growth on a surface front in a two-layer geostrophic current. *J. Mar. Res.* **42**, 761–785.

Ma, Y. C. 1978 The complete solution of the long-wave–short-wave resonance equations. *Stud. Appl. Maths* **59**, 201–221.

Newell, A. C. 1974 Envelope equations. In *Nonlinear Wave Motion*. Lectures in Applied Mathematics, vol. 15, pp. 171–191. American Mathematical Society.

Olson, D. B., Schmitt, R. W., Kennelly, M. & Joyce, T. M. 1985 A two layer diagnostic model of the long-term physical evolution of warm core ring 82B. *J. Geophys. Res.* **90**, 8813–8822.

Paldor, N. 1983*a* Linear stability and stable modes of geostrophic fronts. *Geophys. Astrophys. Fluid Dyn.* **24**, 299–326.

Paldor, N. 1983*b* Stability and stable modes of coastal fronts. *Geophys. Astrophys. Fluid Dyn.* **27**, 217–228.

Paldor, N. 1987 Nonlinear waves on a coupled density front. *Geophys. Astrophys. Fluid Dyn.* **37**, 171–191.

Paldor, N. & Ghil, M. 1990 Finite-wavelength instabilities of a coupled density front. *J. Phys. Oceanogr.* **20**, 114–123.

Paldor, N. & Killworth, P. D. 1987 Instabilities of a two-layer coupled front. *Deep-Sea Res.* **34**, 1525–1539.

Pavia, N. 1992 The breakup of frontal filaments. *J. Phys. Oceanogr.* **22**, 399–403.

Pedlosky, J. 1987 *Geophysical Fluid Dynamics*. Springer.

Phillips, N. A. 1963 Geostrophic motion. *Rev. Geophys.* **1**, 123–176.

Reszka, M. K. & Swaters, G. E. 1999 Eddy formation and interaction in a baroclinic frontal geostrophic model. *J. Phys. Oceanogr.* **29**, 3025–3042.

Rhines, P. B. 1975 Waves and turbulence on a beta-plane. *J. Fluid Mech.* **69**, 417–443.

Robinson, A. R. (ed.) 1983 *Eddies in Marine Science*. Springer.

Roden, G. I. 1975 On North Pacific temperature, salinity, sound velocity and density fronts and their relation to the wind energy flux fields. *J. Phys. Oceanogr.* **5**, 557–571.

Slomp, C. G. 1995 On the Hamiltonian structure, stability characteristics and finite amplitude evolution of geostrophic fronts. MSc thesis, Department of Mathematical Sciences, University of Alberta.

Slomp, C. G. & Swaters, G. E. 1997 Finite amplitude perturbations and modulational instability of a stable geostrophic front. *Geophys. Astrophys. Fluid Dyn.* **86**, 149–172.

Spall, M. A. 1995 Frontogenesis, subduction, and cross front exchange at upper ocean fronts. *J. Geophys. Res.* **100**, 2543–2557.

Stammer, D. 1997 Global characteristics of ocean variability from regional TOPEX/POSEIDON altimeter measurements. *J. Phys. Oceanogr.* **27**, 1743–1769.

Swaters, G. E. 1991 On the baroclinic instability of cold-core coupled density fronts on a sloping continental shelf. *J. Fluid Mech.* **224**, 361–382.

Swaters, G. E. 1993*a* Nonlinear stability of intermediate baroclinic flow on a sloping bottom. *Proc. R. Soc. Lond.* A **442**, 249–272.

Swaters, G. E. 1993*b* On the baroclinic dynamics, Hamiltonian formulation and general stability characteristics of density-driven surface currents and fronts over a sloping continental shelf. *Phil. Trans. R. Soc. Lond.* A **345**, 295–325.

Swaters, G. E. 1998 Numerical simulations of the baroclinic dynamics of density-driven coupled fronts and eddies on a sloping bottom. *J. Geophys. Res.* **103**, 2945–2961.

Tang, B. & Cushman-Roisin, B. 1992 Two-layer geostrophic dynamics. Part II: Geostrophic turbulence. *J. Phys. Oceanogr.* **22**, 128–138.

Verdiére, A. C. de 1986 On mean flow instabilities within the planetary geostrophic equations. *J. Phys. Oceanogr.* **16**, 1981–1984.

Whitham, G. B. 1974 *Linear and Nonlinear Waves*. Wiley.

Williams, G. P. & Yamagata, T. 1984 Geostrophic eddies, intermediate solitary vorticities and Jovian eddies. *J. Atmos. Sci.* **41**, 453–478.

Yamagata, T. 1982 On nonlinear planetary waves: a class of solutions missed by the traditional quasigeostrophic approximation. *J. Oceanogr. Soc. Japan* **38**, 236–244.